HHS Public Access

Author manuscript

Dev Cell. Author manuscript; available in PMC 2017 August 24.

Published in final edited form as:

Dev Cell. 2017 March 27; 40(6): 566–582.e5. doi:10.1016/j.devcel.2017.03.001.

miR-219 Cooperates with miR-338 in Myelination and Promotes Myelin Repair in the CNS

Haibo Wang[1], **Ana Lis Moyano**[2], **Zhangyan Ma**[1], **Yaqi Deng**[1], **Yifeng Lin**[3], **Chuntao Zhao**[1], **Liguo Zhang**[1], **Minqing Jiang**[1], **Xuelian He**[1], **Zhixing Ma**[1], **Fanghui Lu**[1], **Mei Xin**[1], **Wenhao Zhou**[3], **Sung Ok Yoon**[4], **Ernesto R. Bongarzone**[2,5], and **Q. Richard Lu**[1,3,6,*]

[1]Division of Experimental Hematology and Cancer Biology, Department of Pediatrics, Cincinnati Children's Hospital Medical Center, Cincinnati, OH 45229, USA

[2]Department of Anatomy and Cell Biology, University of Illinois at Chicago, Chicago, IL 60612, USA

[3]Key Laboratory of Birth Defects, Children's Hospital of Fudan University, Shanghai 201102, China

[4]Department of Molecular and Cellular Biochemistry, Center for Molecular Neurobiology, The Ohio State University, Columbus, OH 43210, USA

[5]Departamento de Química Biologica, Facultad de Farmacia y Bioquímica, Universidad de Buenos Aires, Argentina

SUMMARY

A lack of sufficient oligodendrocyte myelination contributes to remyelination failure in demyelinating disorders. miRNAs have been implicated in oligodendrogenesis; however, their functions in myelin regeneration remained elusive. Through developmentally regulated targeted mutagenesis, we demonstrate that *miR-219* alleles are critical for CNS myelination and remyelination after injury. Further deletion of *miR-338* exacerbates the miR-219 mutant hypomyelination phenotype. Conversely, miR-219 overexpression promotes precocious oligodendrocyte maturation and regeneration processes in transgenic mice. Integrated transcriptome profiling and biotin-affinity miRNA pull-down approaches reveal stage-specific miR-219 targets in oligodendrocytes and further uncover a novel network for miR-219 targeting of differentiation inhibitors including Lingo1 and Etv5. Inhibition of Lingo1 and Etv5 partially rescues differentiation defects of *miR-219*-deficient oligodendrocyte precursors. Furthermore, miR-219 mimics enhance myelin restoration following lysolecithin-induced demyelination as well as experimental autoimmune encephalomyelitis, principal animal models of multiple sclerosis.

[*]Correspondence: richard.lu@cchmc.org.
[6]Lead Contact

SUPPLEMENTAL INFORMATION

Supplemental Information includes eight figures, five tables, and one movie and can be found with this article online at http://dx.doi.org/10.1016/j.devcel.2017.03.001.

AUTHOR CONTRIBUTIONS

Conceptualization and Methodology, Q.R.L., E.R.B., H.W., and Zhangyan Ma; Investigations, H.W., A.L.M., Zhangyan Ma, Y.D., Y.L., C.Z., L.Z., M.J., X.H., Zhixing Ma, F.L., and M.X.; Writing — Original Draft, H.W. and Q.R.L.; Writing — Review & Editing, H.W., A.L.M., M.X., S.O.Y., W.Z., E.R.B., and Q.R.L.; Funding Acquisition, Q.R.L. and E.R.B.

Together, our findings identify context-specific miRNA-regulated checkpoints that control myelinogenesis and a therapeutic role for miR-219 in CNS myelin repair.

Graphical abstract

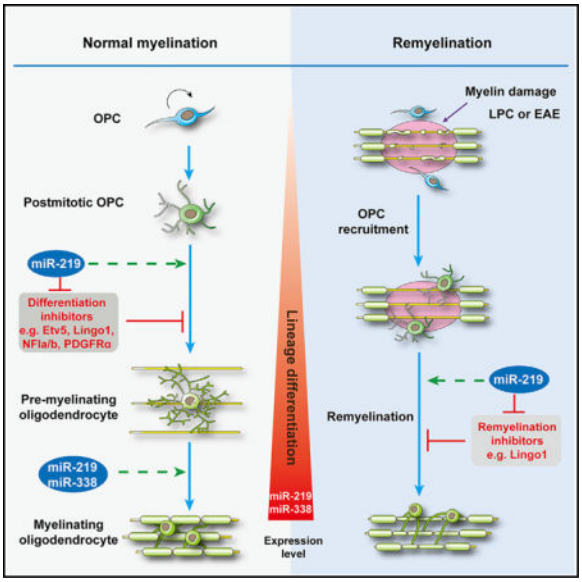

INTRODUCTION

Myelin formed by oligodendrocytes (OLs) in the vertebrate CNS insulates axons to promote rapid, energy-efficient action potential propagation. A failure in myelin repair after OL damage contributes to persistence of demyelination in debilitating diseases such as multiple sclerosis (MS) and leukodystrophies (Franklin and Gallo, 2014). At present, the molecular mechanisms that hinder OL regeneration and remyelination are not fully understood. A balance of opposing extracellular signaling activities and intracellular regulators has been shown to orchestrate OL precursor (OPC) differentiation in a spatially and temporally specific manner (Emery et al., 2009; Gallo and Deneen, 2014). Activation of the inhibitory pathways including BMP, Notch, Wnt, and Lingo1 signaling (Fancy et al., 2009; Mi et al., 2007; Sabo et al., 2011; Ye et al., 2009; Zhang et al., 2009) and transcriptional regulators including Nfia (Glasgow et al., 2014) inhibits remyelination in animal models of MS. Blocking these inhibitory factors is an attractive therapeutic approach to promote myelin repair.

MicroRNAs (miRNAs), a class of short non-coding RNAs with ~22 nucleotides, regulate a multitude of biological processes by blocking translation of mRNAs through targeting their untranslated and coding regions (Bartel, 2009; Rigoutsos, 2009; Stefani and Slack, 2008). Recent studies suggests that mRNA degradation rather than translational inhibition is a major mechanism for miRNA-mediated target inhibition (Guo et al., 2010). By controlling multiple aspects of cellular development and homeostasis, including cell-fate determination and differentiation, miRNAs are powerful post-transcriptional regulators (Bartel, 2009; He et al., 2012; Inui et al., 2010). Global abrogation of miRNA maturation by deletion of *Dicer1*

encoding the miRNA-processing enzyme severely compromises OL differentiation and myelination (Dugas et al., 2010; Shin et al., 2009; Zhao et al., 2010). A cohort of miRNAs has been identified that modulate OL differentiation in vitro (Dugas et al., 2010; Lin and Fu, 2009; Zhao et al., 2010). Among them, miR-219 and miR-338 are preferentially and abundantly expressed in mature OLs (Dugas et al., 2010; Lau et al., 2008; Zhao et al., 2010). Both miRNAs are evolutionary conserved in vertebrate genomes from fish to humans. In addition, chronic MS lesions are essentially devoid of miR-219 and miR-338 (Junker et al., 2011), suggesting a potential role for these miRNAs in the remyelination process. In vitro culture studies suggest that miR-219 is critical for OPC differentiation and acts through suppressing expression of OL differentiation inhibitors, including PDGFRα, Sox6, and Zfp238, predicted by computational algorithms (Dugas et al., 2010; Zhao et al., 2010); however, in vivo functions of these miRNAs and their context-specific targets remain elusive.

Given that many of the miRNA functions observed in vitro could not be recapitulated in vivo, the functions of miRNAs such as miR-219 in myelination and remyelination have not been defined in vivo. In addition, whether their mRNA targeting is stage dependent remains undetermined. Our present gain-and loss-of-function studies demonstrate a critical role for *miR-219* in OL differentiation and remyelination in vivo. By analyzing miR-219-regulated transcriptome profiles and direct targets, we identify a novel miR-219-targeted inhibitory network. Furthermore, augmentation of miR-219 enhances myelin restoration in different animal models of MS including toxin-induced demyelination and experimental autoimmune encephalomyelitis (EAE), suggesting a therapeutic role for miR-219 in promoting myelin repair in demyelinating diseases in the CNS.

RESULTS

Deletion of *miR-219* Genes Leads to OL Differentiation Defects in the Developing CNS

miR-219 is encoded by *miR-219-1* and *miR-219-2* genes, which are located on chromosome 17 and chromosome 2, respectively, in the mouse genome. Identical mature miR-219 is produced from both *miR-219-1 and miR-219-2*. To study the function of miR-219 in vivo, we generated mutant mice harboring floxed *miR-219-1* or *miR-219-2* alleles through homologous recombination in embryonic stem cells (Figures 1A and 1B). The floxed *miR-219-1* and *miR-219-2* mice were bred with a CAG-Cre line (Sakai and Miyazaki, 1997) to remove the floxed alleles in the germline and generate *miR-219-1*$^{-/-}$, *miR-219-2*$^{-/-}$, and *miR-219-1/2*$^{-/-}$, the latter lacking both *miR-219* alleles (Figures 1C–1E).

Individual *miR-219-1* and *miR-219-2* null mice were born at Mendelian ratios. *miR-219-1*$^{-/-}$, mice were phenotypically similar to wild-type mice, whereas *miR-219-2*$^{-/-}$ mice developed tremors at adulthood. Strikingly, the majority of *miR-219-1/2*$^{-/-}$ double-null animals died around birth. In *miR-219-1/2*$^{-/-}$ double mutants, expression of *miR-219* was essentially undetectable (Figure 1F). Deletion of *miR-219-1* did not significantly alter the total level of mature miR-219 in the OL-enriched optic nerves, whereas the level of mature miR-219 was significantly reduced in *miR-219-2*$^{-/-}$ mice (Figure 1F), suggesting that expression from *miR-219-2* is a main contributor to total miR-219 levels.

To evaluate OL development in *miR-219* single and double mutants, we examined expression of mature OL markers *Mbp* (myelin basic protein) and *Plp1* (proteolipid protein) by in situ hybridization in the spinal cord. *Mbp* and *Plp1* expression was comparable in *miR-219-1*$^{-/-}$ and wild-type mice at P0 (postnatal day 0) but was reduced in *miR-219-2*$^{-/-}$ mice and was further diminished in *miR-219-1/2*$^{-/-}$ mutants (Figures 1G and 1H). In contrast, expression of *PDGFRα*, a marker for OPCs, did not appear to be substantially altered in either *miR-219* single or double mutants relative to wild-type animals (Figures 1G and 1I). We did not detect substantial cell death assayed by the active cleaved form of caspase-3 in *miR-219* knockouts (data not shown), suggesting that *miR-219* deficiency does not affect OPC formation, but inhibits their differentiation during development.

Recently, miR-219 was found to regulate neural precursor cell differentiation in zebrafish (Hudish et al., 2013). In contrast, we did not detect substantial alterations in expression of the OL specification factor Olig2, and neurogenesis-associated factors such as Pax6, Tuj1, and Islet1 in the developing spinal cord or brain of *miR-219-1/2*$^{-/-}$ embryos (Figure S1 and data not shown), indicating that *miR-219* deletion does not impair neural differentiation substantially in the murine CNS.

miR-219 Ablation in Oligodendrocyte Lineage Cells Impairs CNS Myelination

Due to the neonatal lethality of *miR-219-1/2* null mice that precludes analysis of postnatal myelinogenesis, we generated conditional *miR-219* mutants by breeding *miR-219-1*$^{fl/fl}$ and *miR-219-2*$^{fl/fl}$ mice with an OL lineage-expressing *Olig1-Cre* line (Xin et al., 2005; Ye et al., 2009) (Figure 2A). *miR-219-1*$^{fl/fl}$; *Olig1-Cre*$^{+/-}$ (*miR-219-1*-cKO), *miR-219-2*$^{fl/fl}$*;Olig1-Cre*$^{+/-}$ (*miR-219-2-cKO*), *miR-219-1/2*$^{fl/fl}$*;Olig1-Cre*$^{+/-}$ (*miR-219-dCKO*) and double-heterozygous control (*miR-219-1*$^{fl/+}$/2$^{fl/+}$*;Olig1-Cre*$^{+/-}$) mice were born at predicted Mendelian ratios. Cre-mediated excision of the *miR-219-1/2*$^{fl/fl}$ alleles efficiently abrogated *miR-219-1/2* expression in the spinal cord (Figure 2B) assessed by qRT-PCR at P7. The *miR-219-dCKO* mice developed tremors beginning around postnatal week 3, the peak period of myelinogenesis, and exhibited severe seizures as well as ataxia in adulthood (Figure 2C; Movie S1). Most *miR-219*-dCKO mice died around 4 months of age (Figure 2D).

In situ hybridization analysis of the cortex, corpus callosum, and spinal cord at P7 and at P28 indicated that expression of *Mbp* and *Plp1* was substantially diminished in *miR-219*-dCKO mice (Figures 2E and 2F). Similarly, in the optic nerve, corpus callosum, and cortex of *miR-219*-dCKO mice at postnatal stages, there was a striking reduction in the number of CC1^{+} mature OLs (Figures 2G–2I and 2K), consistent with the expression correlation between *miR-219* and the mature OL marker *Plp1* in different CNS regions (Figure S2A). By contrast, the number of OPCs marked by NG2 was comparable between control and mutant mice (Figures 2I and 2J). We did not detect substantial alterations in the expression pattern of GFAP and NeuN, the markers for astrocytes and neurons, respectively, in the *miR-219*-dCKO brain (Figures S2B–S2D). The dCKO mice exhibited more severe defects in MBP and CC1 expression in the cortex than did single *miR-219-1* or 2-cKO mice (Figure S2E). Consistent with the *miR-219-2* null phenotype and its impact on miR-219 dosage (Figure 1), the *miR-219-2*-cKO mice also developed dysmyelination albeit to a reduced extent compared with *miR-219*-dCKO mice (Figure S2E).

To confirm myelination deficits, we further examined myelin sheath assembly in *miR-219*-dCKO mice by electron microscopy (EM). At P28, there were significantly fewer myelinated axons in the optic nerve and spinal white matter of *miR-219*-dCKO mice than controls (Figures 2L–2P). In addition, the myelin *g* ratio, which is inversely proportional to myelin thickness, in *miR-219*-dCKO optic nerves and spinal cords, was significantly higher than their controls (Figures 2N and 2Q). This indicates thinner myelin sheaths formed around the axons in the CNS of *miR-219*-deficient mice.

Very few mutant mice were able to survive beyond 6 months of age (Figure 2D). We analyzed the gross structure of myelination in these rare survivors and found that compromised expression of *Mbp* and *Plp1* persisted in the cortices of *miR-219*-dCKO mice at P215 (Figure S2F). Similarly, the percentage of myelinated axons and myelin thickness in the mutant spinal cord remained significantly lower at P215 (Figures 2R–2T), indicating that myelin deficits persist throughout the lifespan of *miR-219*-dCKO mutant mice.

miR-338 Deletion Exacerbates the Dysmyelination Phenotype in *miR-219* Mutants

Like miR-219, miR-338 is abundantly expressed in mature OLs (Dugas et al., 2010; Lau et al., 2008; Zhao et al., 2010). We generated mutant mice harboring *miR-338 floxed* alleles on chromosome 11 through homologous recombination. *miR-338* floxed alleles were further removed by the germ-cell-expressing CAG-Cre line to generate *miR-338*$^{-/-}$ mice (Figures 3A–3C). In stark contrast to the neonatal lethality observed in *miR-219*$^{-/-}$ mice, *miR-338*$^{-/-}$ mice were born at the normal Mendelian ratio and were phenotypically similar to wild-type mice. In the developing brain and spinal cord at P30, expression of OL markers MBP and CC1 as well as the OPC marker PDGFRα was comparable between control and *miR-338*$^{-/-}$ mice (Figures 3D–3F), suggesting that miR-338 is dispensable for normal OL myelination in the CNS.

To explore more fully the role of miR-338 in OL maturation, we then bred *miR-338*$^{-/-}$ mice with *miR-219*-dCKO mice to generate *miR-219*-dCKO;*miR-338* triple knockout (tKO) mice. The level of MBP and the number of CC1^{+} cells in the cortices of the tKO mice were further reduced compared with counterparts in *miR-219*-dCKO mice (Figures 3D and 3E), despite comparable abundance of PDGFRα^{+} OPCs (Figure 3F). Similarly, expression of *Mbp* and *Plp1* in the spinal cord was reduced in *miR-219/338* tKO mice compared with *miR-219*-dCKO mice (Figures 3G and 3H). These observations suggest that miR-219 and miR-338 cooperate to regulate the full extent of OL maturation.

miR-219 Is Required for OL Remyelination after Demyelination

Given the essential role of miR-219 in normal myelination, we hypothesized that miR-219 is required for remyelination after injury. We utilized an experimental demyelinating model induced by injection of lysolecithin (LPC), which causes acute demyelinating injury followed by spontaneous myelin repair (Franklin, 2002). The myelin regeneration process begins with an OPC proliferation/recruitment phase approximately 7 days post LPC lesions (dpl 7) and a remyelinating phase around dpl 14 (Franklin, 2002). Expression of miR-219 and miR-338 is upregulated over the remyelination phase after LPC-induced demyelination (Figures 4A and S3A). To address the role of *miR-219* in remyelination after injury at

adulthood, we generated an *miR-219*-inducible knockout by breeding *miR-219-1/2*$^{lox/lox}$ mice with a tamoxifen-inducible OL-expressing *Plp-CreERt* line (Doerflinger et al., 2003) carrying a Rosa26-tdTomato reporter, which labels the cells having undergone Cre-mediated recombination of *miR-219* floxed alleles.

Tamoxifen was administered at 5 days prior to LPC injection to delete *miR-219-1/2* in 8-week old *miR-219-1/2*$^{lox/lox}$*:Plp-CreERt*^{tdTomato} mice (referred to as *miR-219*-iKO) and heterozygous mice *miR-219-1/2*$^{lox/+}$*:Plp-CreERt*^{tdTomato} as controls. Tamoxifen-induced *miR-219* ablation in OLs at adult stages did not affect myelin maintenance in the spinal cords of *miR-219*-iKO mice (Figures S3B and S2C). LPC was then injected into the ventral white matter of the spinal cord, which was followed by administration of tamoxifen for an additional 5 days, and harvested at different time points (Figure 4B).

There were significantly fewer *Mbp*- and *Plp1*-expressing OLs in spinal cords of *miR-219*-iKO mice at dpl 8and 15 than controls (Figures 4C and 4D). The number of *PDGFRα*-expressing OPCs was higher in *miR-219*-iKO than in control mice at dpl 15, although OPC recruitment was comparable between control and iKO mice at dpl 8 (Figures 4C and 4E). Conversely, there were fewer CC1$^+$ differentiating OLs in the lesions of *miR-219*-iKO at dpl 15 and 21 (Figures 4F–4H). At dpl 30, CC1$^+$ OLs in the lesions of *miR-219*-iKO animals approached but did not match those in controls (Figure 4I). The percentage of myelinated axons was substantially reduced in the lesions of *miR-219*-iKO mice at dpl 15 (Figures 4J and 4K). Newly generated myelin sheaths around axons as assessed by *g* ratios were significantly thinner in *miR-219*-iKO mice (Figure 4L). These data suggest that miR-219 is critical for remyelination after demyelination.

miR-219 Overexpression Promotes OL Maturation and Remyelination

To determine whether overexpression of *miR-219* could promote OL maturation in vivo, we generated transgenic mice (*miR-219*-Tg) that express miR-219-2 and a GFP reporter under the control of an OL-expressing *Cnp1* promoter (Gravel et al., 1998). Expression of miR-219 in the corpus callosum of these *miR-219*-Tg mice at P7 was approximately 3-fold higher in the transgenic mice than in age-matched wild-type animals, yet comparable at the adult stage P50 (Figure 5A). GFP was mainly detected in CC1$^+$ OLs of transgenic mice (Figure 5B). Although there were very few MBP$^+$ OLs in the cortices of wild-type mice at P3, we detected an extensive amount of MBP$^+$ cells in *miR-219*-Tg animals (Figure 5C). The similar corroborating phenotypes observed in three additional *miR-219*-Tg transgenic lines (data not shown) suggest that overexpression of *miR-219* promotes OL maturation.

Despite the substantially higher number of MBP$^+$ cells in the cortex of neonatal stages, at the adult stage, the percentage of myelinated axons and the myelin *g* ratio (Figures 5D and 5E), as well as the number of CC1$^+$ OLs and PDGFRα$^+$ OPCs (Figures S4A and S4B), were comparable between *miR-219*-Tg and wildtype mice, which is consistent with their comparable levels of miR-219 (Figure 5A). Given the similar myelination profiles between adult wild-type and *miR-219*-Tg mice, we then examined the effects of *miR-219* overexpression during myelin repair by subjecting the animals to LPC-induced demyelinating injury. At dpl 7, the number of PDGFRα$^+$ OPCs and their proliferation rate in LPC-lesioned spinal cords was comparable between wild-type and *miR-219*-Tg mice

(Figures 5F–5H). At dpl 14, we found that there were significantly more $CC1^+$ OLs in the lesions of *miR-219*-Tg than in wild-type mice, while the number of $PDGFR\alpha^+$ OPCs was reduced (Figures 5J and 5K), and the total number of OPCs and OLs was comparable between control and *miR-219*-Tg mice (Figure 5L). Given that the transgene reporter expression was detected in OPCs in lesions (Figure S4C), *Cnp1*-driven miR-219 expression promotes differentiation of OPCs and $Cnp1^+$ postmitotic OPCs in the demyelinating lesions. The percentage of remyelinated axons and the thickness of newly formed myelin sheaths in the lesions of *miR-219*-Tg mice were significantly higher than controls (Figure 5M–5O), suggesting that elevation of miR-219 levels enhances the OL capacity to remyelinate in the demyelinating lesion.

miR-219 Targets Stage-Specific Inhibitors to Promote OL Differentiation

Previous studies identified a few miR-219 targets using mainly target prediction programs that lack context specificity (Dugas et al., 2010; Zhao et al., 2010). To identify mRNAs regulated by miR-219 during OL development, we performed RNA-seq transcriptome profiling analysis of the optic nerve, an OL-enriched white matter tract, in control and *miR-219*-dCKO animals at P12. *miR-219* deletion led to a downregulation of myelination-regulatory genes such as *Sox10*, *Myrf*, and *Zeb2/Sip1* and myelin-associated genes such as *Cnp*, *Mag*, and *Mobp* (Figures 6A and 6B; Table S1), consistent with the dysmyelination phenotype in *miR-219*-dCKO mice. Among the upregulated genes in *miR-219* mutants, we identified previously validated miR-219 targets, including *Elovl7* and *Zfp238* (Dugas et al., 2010; Zhao et al., 2010). To further identify the miR-219-targeted transcription factors, we analyzed the transcriptional regulatory genes upregulated in *miR-219* mutants using the miRNA target prediction programs TargetScan and miRBase (Bartel, 2009; Grimson et al., 2007; Krek et al., 2005). In addition, the RNAhybrid program was used to calculate the free energy of miRNA/target duplex formation (Rehmsmeier et al., 2004). These analyses support that genes encoding transcriptional regulators *Etv5, Nfib, Pbx1*, and *Nfia* are candidate targets of miR-219 (Figure 6C).

To determine differences in miR-219 target mRNAs as a function of differentiation stages, we transfected rat OPCs or differentiating immature OLs (iOL) with the miR-219 mimic or the control miRNA and used RNA-seq to profile transcriptomes. Gene ontology (GO) analysis indicated that genes downregulated in OPCs after miR-219 treatment were significantly associated with neurogenesis (Figure 6D), whereas those downregulated in immature OLs were related to mitotic cell division (Figure 6E). These observations suggest that miR-219 targets distinct sets of genes at different stages of OPC maturation by both suppressing proliferation and alternative fates of OPCs, as well as enhancing cell-cycle exit and terminal differentiation.

We inferred candidate miRNA target genes from opposite regulation under the ablation and overexpressed conditions, such that expression of the target should increase upon miRNA ablation and conversely decrease upon miRNA overexpression. When comparing the genes downregulated in miR-219-transfected OPCs with those upregulated in *miR-219*-deficient optic nerves, we identified approximately 24 common candidate targets at this OPC stage (Table S2), including *Nfib* and *Nfia*, which act as an inhibitor of OPC fate specification and

differentiation (Deneen et al., 2006; Glasgow et al., 2014). In addition, the gene sets common between downregulated genes in miR-219-transfected iOLs under differentiation conditions and those upregulated in *miR-219*-deficient optic nerves include approximately 67 putative miR-219 target genes (Table S3), including a transcriptional regulator Etv5, which is associated with the specification of astrocyte precursors (Li et al., 2012).

Overexpression of miR-219 significantly reduces expression of *Nfia* and *Nfib* in OPCs or *Etv5* under differentiating conditions (Figure 6F). There are two predicted miR-219 binding sites in the 3′ UTR of *Nfia*, two in the coding region of *Nfib*, and one in the coding region of *Etv5* (Figures S5A and S5B). We verified that miR-219 suppresses expression of these genes using an miRNA target reporter assay (Zhao et al., 2010) (Figure S5C). Furthermore, mutation of the miR-219 "seed" sequence in the putative targeted segments of these reporter genes abolished the miR-219-dependent inhibition of reporter gene expression (Figures S5B and S5C).

Nfia/b has been shown to inhibit expression of myelination-promoting genes such as *Mbp, Olig2*, and *Sox10* to block OL differentiation (Fancy et al., 2012; Glasgow et al., 2014); however, the functions of *Etv5* in OL differentiation have not been fully characterized. Enforced expression of *Etv5* led to significant reductions in the number of mature MBP^+ OLs among transfected OPCs (Figures S5D and S5E). Furthermore, overexpression of *Etv5* suppressed expression of myelination-associated genes, including *Mbp*, *Plp1, Cnp*, and *Myrf*, but did not affect *PDGFRα* or *Id2* expression (Figure S5F). Conversely, knockdown of *Etv5* led to a significant increase in the number of mature MBP^+ OLs among transfected OPCs (Figures S5G and S5H). These observations suggest that the miR-219 target, Etv5, acts as an inhibitor for OPC differentiation.

miR-219 Targets and Inhibits Lingo1, an Inhibitor of OL Myelination

To identify mRNAs directly targeted by miR-219, we used a biotinylated miRNA-mRNA pull-down approach (Lal et al., 2011; Orom and Lund, 2007). We transfected primary rat OPCs with biotinylated miR-219 or cel-miR-67, a negative control, which has minimal sequence identity with miRNAs in mammals (Xin et al., 2012). mRNAs pulled down by biotinylated miR-219 or the control miRNA were subject to RNA-seq analysis (Figure S5I). Transcripts with both an enrichment ratio exceeding 3-fold for biotinylated miR-219 pull-downs over input controls together with downregulation exceeding 25% in OPCs that overexpress miR-219 were considered candidate targets of miR-219 (Table S4). Among the candidate target mRNAs, we identified previously identified miR-219 targets such as *PDGFRα* and *Sox6*. In addition, *Lingo1*, which encodes a potent inhibitor of myelination (Mi et al., 2007), was identified as a candidate miR-219 target with the highest enrichment score (Table S4). Subsequent over-expression of miR-219 in OPCs confirmed that *Lingo1* was downregulated by miR-219 (Figure 6G).

Lingo1 contains two putative miR-219 binding sites within its coding region (Figure S5B). To validate the direct targeting of *Lingo1* transcript by miR-219, we constructed a luciferase reporter carrying a *Lingo1* cDNA segment that includes the two predicted miR-219 binding sites and a reporter with both seed sequences mutated. Overexpression of miR-219 significantly reduced the activity of the reporter carrying the wild-type *Lingo1* segment, and

this effect was abolished in the reporter carrying the mutant *Lingo1* segment (Figure 6H), suggesting that these binding sites in the *Lingo1* mRNA are directly targeted by miR-219. We further showed that Lingo1 protein expression was substantially reduced in OPCs transfected with miR-219 (Figure 6I). Together with upregulation of *Lingo1* in *miR-219*-dCKO optic nerves (Figures 6A and 6B), our data suggest disinhibition of Lingo1 expression in the absence of miR-219 in vivo.

Lastly, we tested whether inhibition of Lingo1 expression rescues the differentiation defects of *miR-219*-deficient OPCs. Under differentiation conditions, wild-type OPCs differentiated into MBP^+ OLs, whereas *miR-219*-deficient OPCs exhibited a significantly reduced differentiation capacity (Figures 6K and 6L). In addition, knockdown of *Lingo1* or *Etv5*, an miR-219 target in differentiating OL, using siRNAs significantly increased the formation of MBP^+ mature OLs in *miR-219*-deficient cells (Figures 6K and 6L). The morphology of these MBP^+ cells, however, reflected an intermediate stage rather that of fully mature OLs, suggesting that further signals are needed for complete morphologic maturation. Moreover, silencing of both *Lingo1* and *Etv5* further increased the number of MBP^+ OLs with more elaborated processes and myelin gene expression compared with knockdown of either *Lingo1* or *Etv5* alone in *miR-219*-deficient OPCs (Figures 6K–6M). Thus, suppression of *Lingo1* and *Etv5* rescues, at least partially, the differentiation defects of *miR-219*-deficient OPCs, suggesting that miR-219 exerts some of its effects through lowering Lingo1 and Etv5 levels.

miR-219 Mimic Promotes Remyelination after Lysolecithin-Induced Demyelinating Injury

To further investigate the clinical relevance of miR-219 in myelin repair, miR-219 mimic or control miRNA was delivered to LPC-demyelinating lesions through co-infusion. Delivery was demonstrated by infusion of Cy3-conjugated miRNA mimic at the time of LPC injection (Figure 7A). The mice were subsequently treated intrathecally with miR-219 mimic or control miRNA once daily starting at the time of LPC injection and thereafter for 4 consecutive days. The injured spinal cord segments were evaluated at different time points. We observed significantly higher levels of *Mbp* expression and more *Plp1*$^+$ differentiating OLs in the lesions of the mice treated with miR-219 mimic than in those treated with control miRNA at dpl 8 and 14 (Figures 7B–7D). While the overall density of $Olig2^+$ OLs was similar between the treatments, the number of $CC1^+$ differentiating OLs was increased, whereas $PDGFR\alpha^+$ OPCs were reduced in the lesions treated with miR-219 mimic compared with controls at dpl 14 (Figures 7E–7H). As controls, we did not detect any significant alteration in the number of $CC1^+$ OLs, $PDGFR\alpha^+$ OPCs, or apoptotic loss of OPCs in the vehicle-injected uninjured spinal cord of wild-type adult mice treated with miR-219 mimic (Figures S6A–S6C).

Ultrastructural analysis of LPC lesions indicated that the percentage of remyelinated axons and the thickness of newly formed myelin sheaths in the lesions of mice treated with the miR-219 mimic were significantly higher than in mice treated with the control miRNA (Figures 7I–7K). A similar demyelinating paradigm using LPC-induced demyelination in the corpus callosum showed that intranasal administration of miR-219 increased $CC1^+$ OL numbers (Figures 7L and 7M) and MBP expression (Figures S6D–S6F), consistent with

enhanced OL differentiation with miR-219-enriched exosome treatment in a slice culture (Pusic and Kraig, 2014). These observations suggest that elevation of miR-219 levels promotes myelin regeneration in the CNS in vivo.

miR-219 Augments the Recovery of Neurological Functions in EAE Mice

To evaluate the potential impact of miR-219 as a therapeutic agent in immune-mediated demyelination, we used an MOG35-55-induced EAE animal model (Bittner et al., 2014). This model recapitulates many clinical and pathological features of human MS, including inflammatory responses, progressive demyelination, and axonal loss (Bruck, 2005). Eight-week-old female C57BL/6 mice immunized with MOG35-55 were treated with control miRNA and miR-219 mimic via intrathecal administration starting at post-immunization day (PID) 19, when symptoms indexed by mean EAE clinical score peaked. The control-treated mice exhibited chronic hindlimb paresis over the treatment period (Figure 8A). In contrast, the animals treated with miR-219 mimics exhibited a significant improvement in motor function, regaining use of both hind limbs (Figure 8A). Functional recovery in miR-219-treated mice was correlated positively with histological improvements, including restoration of MBP expression in the lesions of lumbar spinal cords, which exhibit the prominent demyelinating lesions in EAE (Lin et al., 2013), and reduction of the demyelinated regions (Figures 8B, 8C, and S7A). The histological and functional improvements appear to be at least in part due to the presence of a higher number of $CC1^+$ or *Plp1*$^+$ OLs in the spinal lesions from miR-219-mimic-treated mice than in controls (Figures 8D–8G). In addition, there was a significant increase in the percentage of remyelinating axons in the demyelinating lesions in miR-219-mimic-treated mice (Figure 8H–8J). Furthermore, in contrast to the prominent axonal loss, axons labeled by Neurofilament M were largely preserved in the spinal lesions of animals treated with miR-219 mimics (Figure 8K). miR-219 mimic treatment did not have a noticeable effect on the number of $Iba1^+$ microglia/macrophages and $CD3^+$ T cells (Figures 8L–8N), as well as $MHCII^+$ M1 microglia, $CD19^+$ B cells, and $Ly6G^+$ neutrophils in the lesions (Figures S7B–S7D). In addition, qPCR analysis showed that miR-219 mimic treatment did not significantly change the expression of immune cytokines in the lumbar spinal cords of EAE mice (Figure S7E). Thus, these data suggest that miR-219 mimic acts as a remyelination-promoting agent to improve the clinical symptoms of EAE.

DISCUSSION

miRNAs as Cell-Intrinsic Regulators of Myelination and Remyelination in the CNS

The absence of effective treatments to counter OL differentiation blocks presents a significant hurdle for remyelination in demyelinating diseases such as MS. Functional dissection of the contributions of small non-coding miRNAs will provide opportunities to safely deploy them as targeted therapeutic agents. In this study, through in vivo targeted loss and gain-of-function studies, we demonstrate that miR-219 is both necessary and sufficient to promote OL myelination and remyelination after demyelination, and further reveal cooperation between miR-219 and miR-338 in OL maturation. Integrative analysis of transcriptome profiles surveying miR-219-regulated genes and direct binding targets uncover stepwise miR-219-mediated silencing in driving OL maturation. Remarkably, although loss-

of-function mutation of most individual miRNAs yields no overt developmental defects in multiple organisms (Miska et al., 2007), the essential role of *miR-219* in myelination indicates that *miR-219* plays a central role in rather than just fine-tuning myelinogenesis. Our findings further highlight the importance of miR-219-mediated post-transcriptional regulation for myelin repair in the CNS.

Our data indicate that individual *miR-219-1* and *miR-219-2* diverge in their ability to compensate for each other's loss despite generating the same mature miRNA. Consistent with the higher abundance of *miR-219-2*, we find that deletion of *miR-219-2* causes myelination deficits, whereas the absence of *miR-219-1* has minimal impact on myelination, indicating a divergent and dose-dependent effect. The *miR-219-1/2* null animals exhibit neonatal lethality, implying that miR-219 might also regulate other essential cellular processes or organismal homeostasis in addition to its function in OL development.

miR-219 deletion in *Plp1*-expressing differentiating OLs caused a defect in remyelination in response to LPC-induced demyelinating injury. miR-219 is mainly expressed in differentiating OLs with a low expression level in OPCs (Dugas et al., 2010; Zhao et al., 2010), the potential function of miR-219 in OPC development and remyelination remains to be determined by utilizing PDGFRα$^+$ OPC-specific Cre lines. Consistent with the fact that *miR-219* overexpression in *Cnp1*$^+$ postmitotic OPCs or immature OL promoted precocious OL maturation during early postnatal development, remyelination efficiency was enhanced considerably in *miR-219*-Tg mice, suggesting that augmentation of miR-219 levels accelerates the onset of the remyelination process.

The dysmyelinating phenotype appears to be more severe in *Dicer1-cKO* mice (Zhao et al., 2010) than in *miR-219*-dCKO mice, suggesting that other miRNAs may yet coordinate with miR-219 to regulate myelination. A possible explanation for this observation may be due to the partial functional redundancy of miR-219 and miR-338. Both are abundant in OLs and regulate a set of differentiation-inhibiting genes such as *Sox6* and *Hes5* (Dugas et al., 2010; Zhao et al., 2010). We showed that mice deficient in both miR-338 and miR-219 have a more severe dysmyelination phenotype than the *miR-219*-dCKO mutant, suggesting that miR-338 and miR-219 have additive effects on OL differentiation and are required for the full extent of myelination.

Stage-Specific Targeting of Differentiation Inhibitors by miR-219 Drives OL Maturation

Previous miR-219 target identification efforts relied mainly on bioinformatics for predictions (Dugas et al., 2010; Zhao et al., 2010). Such algorithms have a high false discovery rate (Alexiou et al., 2009). Cell type and temporally specific miRNA targets cannot be identified using predictive methods. By analyzing transcriptome profile changes caused by *miR-219* deletion in optic nerves and by *miR-219*-overexpression in OPCs and differentiating OLs, we showed that miR-219 targets neurogenic genes or OL differentiation inhibitors such as *Nfia, Nfib*, and *Lingo1* in OPCs and *Etv5* in differentiating OLs. These observations suggest that miR-219 targets distinct sets of genes at different stages to promote OL lineage progression.

Identification of Nfi family members as functional targets of miR-219 is consistent with their inhibitory roles in OL differentiation (Deneen et al., 2006; Fancy et al., 2012; Glasgow et al., 2014). Strikingly, we identify a new miR-219 target, Etv5, during OPC differentiation. Etv5 is a member of the Ets family of transcription factors that are necessary for gliogenesis in *Drosophila*, *Xenopus*, and mice (Kiyota et al., 2007; Klaes et al., 1994; Li et al., 2012). Here, we showed that downregulation of *Etv5* enhances OL differentiation, whereas *Etv5* overexpression repressed OPC differentiation in vitro, suggesting that Etv5 is an inhibitor of OL differentiation. There is no significant alteration in expression of Etv5 upstream regulators such as Mek (Map2k) (Li et al., 2012) and its family members (Map2k1-7) in *miR-219* dCKO mice (data not shown). Furthermore, direct affinity purification of OPC mRNAs that interact with biotin-tagged miR-219 identified a set of miR-219 targets including *Lingo1*, which had not been identified as an miR-219 target based on computational approaches. Inhibition of expression of both *Lingo1* and *Etv5* using siRNA improved the maturation of *miR-219*-deficient OPCs, with inhibition of both more effective than inhibition of either alone. Thus, stage-specific miR-219-mediated antagonism of a Lingo1-Etv5 inhibitory network drives proper timing of OL lineage cell progression.

Par-3 family cell polarity regulators *Pard3* and *Prcki* were identified as targets of miR-219 in zebrafish (Hudish et al., 2013). In transcriptome profiles of *miR-219*-dKO optic nerves, however, we did not detect a substantial alteration in *Pard3* or *Prcki* expression (data not shown). In addition, OL lineage-specific knockout of *Par3 floxed alleles* (Castelli et al., 2013) by *Olig1-Cre* did not yield a detectable alteration in myelination (Figure S8), suggesting a non-essential role of *Par3* in OPC differentiation in mice. These observations suggest that miR-219 targeting is context or species dependent.

miR-219 Targets Differentiation Inhibitory Pathways and Lingo1 for Remyelination

In MS lesions, OPCs are recruited but fail to differentiate into myelinating OLs, suggesting that remyelination is blocked at the differentiation and remyelination stage rather than during OPC recruitment (Chang et al., 2002; Kuhlmann et al., 2008; Wolswijk, 1998). Our in vivo gain- and loss-of-function studies demonstrate that miR-219 is both essential and sufficient for timely remyelination, which is critical for functional recovery as chronic demyelination predisposes to axonal loss in MS. Moreover, delivery of miR-219 mimics into the demyelinating lesions through intrathecal injection or intranasal delivery enhanced CNS remyelination in animal models of demyelinating diseases. We further provide evidence that the miR-219 directly targets and inhibits expression of *Lingo1*, a potent inhibitor of remyelination (Mi et al., 2007). The partial rescue of the differentiation defect in *miR-219*-null OPCs by inhibition of *Lingo1* expression with siRNAs further supports a critical role for miR-219 targeting of Lingo1 in regulating OL differentiation.

During development, expression of a miR-219 target *PDGFRα* (Dugas et al., 2010; Zhao et al., 2010) was unaltered in *miR-219*-null animals while *PDGFRα*$^+$ OPCs increased in the LPC-induced lesions of *miR-219*-deficient animals during the remyelination phase (Figure 4). Given that miR-219 is mainly expressed in differentiated OL during development and adulthood (Dugas et al., 2010; Zhao et al., 2010), these observations suggest that regulation of *PDGFRα* expression by miR-219 is context specific, consistent with the notion that

miRNAs play a critical role especially under pathologic conditions such as injury and stress (Leung and Sharp, 2010; Mendell and Olson, 2012). Since injury stimulates OPC proliferation, it may lead to the accumulation of OPCs, which could undergo apoptosis if they are unable to differentiate. The elevation of miR-219 expression in the accumulated OPCs in demyelinating lesions (Figure S4C) likely down-regulates PDGFRα and promotes OPC differentiation. Although there is a possibility that miR-219 overexpression may potentially reduce the OPC pool, our data suggest that miR-219 likely promotes the differentiation of postmitotic OPCs without significantly intervening OPC proliferation during the proliferation phase after injury.

Functional recovery in MS patients will likely hinge on the therapies that promote myelin regeneration (Deshmukh et al., 2013; Franklin and Gallo, 2014). Chronic human MS lesions are essentially devoid of miR-219 and miR-338 (Junker et al., 2011). Our present studies demonstrate that in vivo delivery of miR-219 enhances OL remyelination not only following toxin-induced acute demyelination but also in immune-mediated chronic demyelination in EAE and improves clinical symptoms in the animal model of MS, indicating the efficacy of miR-219 in myelin repair. At present, we could not exclude the possibility that indirect miR-219 effects on inflammatory cell functions or trafficking, or on the remyelination-independent paracrine glial support of denuded axons, may contribute to functional improvement in EAE mice. Although the OL cell-autonomous function of miR-219 in EAE remains to be determined, the converging outcomes between the LPC-induced and EAE demyelinating animal models suggest the effects of OL-expressing miR-219 on remyelination contribute at least partially to functional improvement. miRNA-based therapeutics have an advantage over antibody therapy such as anti-Lingo1 as miRNAs are more stable (Cho, 2012; Vicente et al., 2016). Since miR-219 targets multiple myelin inhibitory factors in addition to Lingo1, it is conceivable that the augmentation of miR-219 together with other antagonists to myelination inhibitors may provide a multi-point targeting strategy to achieve desired pharmacological effects on promoting timely remyelination in patients with demyelinating diseases such as MS.

STAR⋆METHODS

Detailed methods are provided in the online version of this paper and include the following:

KEY RESOURCES TABLE

REAGENT or RESOURCE	SOURCE	IDENTIFIER
Antibodies		
Rat anti-PDGFRα	BD Bioscience	Cat# 558774; RRID:AB_397117
Rabbit anti-Olig2	Millipore	Cat#AB9610; RRID:AB_10141047
mouse anti-CC1	Calbiochem	Cat#OP80; RRID:AB_2057371
Goat anti-MBP	Santa Cruz	Cat#sc-13914; RRID:AB_648798
Rabbit anti-NeuN	Millipore	Cat#ABN78; RRID:AB_10807945
Mouse anti-GFAP	Sigma	Cat#G3893; RRID:AB_477010

REAGENT or RESOURCE	SOURCE	IDENTIFIER
Rabbit anti-NG2	Millipore	Cat#ab5320; RRID:AB_91789
Rabbit anti-Neurofilament M	Millipore	Cat#AB1987; RRID:AB_91201
Alexa Fluor® 488 Rat anti-CD3	BioLegend	Cat#100212; RRID:AB_493530
Rabbit anti-Iba1	Wako	Cat#019-19741; RRID:AB_839504
Rabbit anti-Lingo1	Millipore	Cat#07-678; RRID:AB_390168
FITC Rat anti-MHCII	BioLegend	Cat#107606; RRID:AB_313321
FITC Rat anti-Ly6G	BioLegend	Cat#127606; RRID:AB_1236494
Mouse anti-O4	Millipore	Cat# MAB345; RRID:AB_94872
Mouse anti-O1	ThermoFisher	Cat# 14-6506-82; RRID:AB_10718397
Mouse anti-Ran2	In this paper	N/A
Biotin mouse anti-CD19	BioLegend	Cat#101504; RRID:AB_312823
Chemicals, Peptides, and Recombinant Proteins		
RIPA buffer	ThermoFisher Scientific	Cat# 89900
Protease inhibitor cocktail	Sigma	Cat#P1860
ECL Western Blotting Substrate	Pierce	Cat#32106
PDGF-AA	PeproTech	Cat#100-13A
bFGF	PeproTech	Cat#100-18B
RNAiMAX	ThermoFisher Scientific	Cat#13778030
TRIzol reagent	ThermoFisher Scientific	Cat#15596018
l-α-lysophosphatidylcholine,	Sigma	Cat#L4129
Tamoxifen	Sigma	Cat#T5648
Corn oil	Sigma	Cat#C-8267
i-Fect	Neuromics	Cat#NI35150
Lipofectamine 2000	ThermoFisher Scientific	Cat#11668027
Streptavidin Sepharose High Performance	GE Healthcare Life Sciences	Cat#17-5113-01
IFA	BD Biosciences	Cat#231131
Tuberculosis (strain H37Ra)	BD Biosciences	Cat#DF3114338
Pertussis toxin 181	List Biological Laboratories	Cat#NC9675592
MOG 35-55	Genemed Synthesis Inc.	Cat#SP-51716-1
Critical Commercial Assays		
Chemiluminescence with the ECL kit	ThermoFisher Scientific	Cat# 34077
iScriptTM cDNA Synthesis Kit	Bio-rad	Cat# 170-8890
Nucleofector Kits	Lonza	Cat# VPI-1006
Bright-Glo reporter assay system	Promega	Cat#E2610
FluoReporter lacZ/Galactosidase Quantitation Kit	ThermoFisher Scientific	Cat#F-2905
GenEdit Site-Directed DNA Mutagenesis Kit	FirstBiotech	Cat#201321
Deposited Data		

REAGENT or RESOURCE	SOURCE	IDENTIFIER
RNA-Seq data	This paper	GEO: GSE80439
Experimental Models: Cell Lines		
Mouse anti-Ran2 hybridoma: B lymphocyte	ATCC	ATCC Number TIB-119
HEK293	ATCC	ATCC Number: CRL-3216
Experimental Models: Organisms/Strains		
miR-219-1/2$^{-/-}$	This paper	N/A
miR-219-1/2$^{fl/fl}$	This paper	N/A
miR-338$^{-/-}$	This paper	N/A
miR-219-Tg	This paper	N/A
Par3 floxed lines	Castelli et al., 2013	N/A
Rosa26^{tdTomato}, Ai14	The Jackson Laboratory	Stock No. 007914
PLP-CreERt	Doerflinger et al., 2003	N/A
Olig1-Cre$^{+/-}$	Xin et al., 2005	N/A
C57BL/6	National Cancer Institute	Strain code:556
Oligonucleotides		
miRVana miRNA Mimic Negative Control #1	ThermoFisher	Cat#:4464058
miR-219 mimic: mmu-miR-219a-5p (miRBase Accession #MIMAT0000664)	ThermoFisher	Cat#:4464066
miRIDIAN microRNA Mimic Negative Control #1 (cel-miR-67)	Dharmacon	Cat#:CN-001000-01-05
Biotin modified miRIDIAN microRNA mmu-miR-219a-5p mimic	Dharmacon	Cat#:C-310578-05-0002
MISSION siRNA Universal Negative Control #1	Sigma	Cat#: SIC001
Mouse Lingo1 siRNA, SASI_Mm01_00137609	Sigma	Cat#:NM_181074
Mouse *Etv5* siRNA, SASI_Mm01_00026515	Sigma	Cat#:NM_023794
Mouse Nfib siRNA,SASI_Mm02_00307243	Sigma	Cat#:NM 001113209
Rat *Lingo1* siRNA, SASI_Rn02_00324112	Sigma	Cat#:XM 001068291
Rat Nfib siRNA, SASI_Rn02_00264790	Sigma	Cat#:NM_031566
See Table S5 for the primers for Genotyping, q-PCR and mutagenesis	N/A	N/A
Recombinant DNA		
pMIR-REPORT miRNA Expression Reporter Vector	ThermoFisher	N/A
pMir-reporter-*Nfia* UTR	This paper	N/A
pMir-reporter-Nfib CD	This paper	N/A
pMir-reporter-*Etv5* CD&UTR	This paper	N/A
pMir-reporter-*Lingo1* UTR	This paper	N/A
pCIG-Nfib	This paper	N/A
pCIG-Etv5	This paper	N/A

REAGENT or RESOURCE	SOURCE	IDENTIFIER
pCIG-miR-219-2	This paper	N/A
Software and Algorithms		
Toppfun	Cincinnati Children's Hospital Medical Center	https://toppgene.cchmc.org/enrichment.jsp
TopHat v2.0.13	Genome Biology 2013 14:R36	http://www.ccb.jhu.edu/software/tophat/index.shtml
R language	R Core Team (2016) The R Project for Statistical Computing	http://www.r-project.org
TopHat	Computational Biology at Johns Hopkins University	http://tophat.cbcb.umd.edu
GraphPad Prism 6.00	GraphPad	www.graphpad.com

CONTACT FOR REAGENT AND RESOURCE SHARING

Further information and requests for resources and reagents should be directed to and will be fulfilled by the Lead Contact, Q. Richard Lu (Richard.lu@cchmc.org).

EXPERIMENTAL MODEL AND SUBJECT DETAILS

Animals—To generate floxed miRNA mutant mice, we inserted two *loxP* sites to flank the *miR-219-1, miR-219-2* or *miR-338* gene region, followed by a neomycin selection and DTA cassette, in the pKO-915 vector (Stratagene, La Jolla, CA). The targeting vector was linearized with *Not*I and electroporated into mouse J1 embryonic stem cells. G418-resistant cells were selected and confirmed by Southern blot analysis. To generate *miR-219* transgenic mice, a 500-bp segment carrying *miR-219-2* gene together with a C-terminal IRES-GFP was inserted after a 4.0-kb *Cnp1* promoter (Gravel et al., 1998), which replaces *Mbp* promoter in the pMG2 vector. All viable founder mice appeared to be fertile and produced similar phenotypes. The data presented are derived from the progeny of a single transgenic line. Mice carrying floxed *miR-219* or *miR-338* alleles were bred with the CAG-Cre line to generate miRNA null mice. *miR-219, miR-338*, or *Par3* floxed lines (Castelli et al., 2013) were crossed with *Olig1-Cre*$^{+/-}$ mice (Xin et al., 2005) to generate *miR-219*-cKO and their heterozygous control mice. *PLP-CreERt* transgenic mice (Doerflinger et al., 2003) and *Rosa26*^{tdTomato} reporter mice (Ai14, JAX Labs) were crossed with floxed *miR-219* mice to generate the OL-specific *miR-219-iKO* mice. Animals of either sex were used in the study and littermates were used as controls unless otherwise indicated. The mouse strains in this study were generated and maintained on a mixed C57Bl/6;129Sv background and housed (three or less animals per cage) ina vivarium with a 12-hour light/dark cycle. All animal studies were approved by the Institutional Animal Care and Use Committee of the Cincinnati Children's Hospital Medical Center, USA.

Cell Culture—Primary rat OPCs were isolated from cortices of pups at P2 using a differential detachment procedure as previously described (Zhao et al., 2016). Isolated rat OPCs were grown in OPC growth medium (Sato medium-supplemented mitogens 10 ng/ml PDGF-AA and 20 ng/ml basic fibroblast growth factor), and differentiated in OL differentiation medium (Sato medium only or supplemented with 15 nM triiodothyronine

and 10 ng/ml ciliary neurotrophic factor). Mouse OPCs were isolated from P5-P6 cortices by immunopanning with antibodies against Ran-2, GalC and O4 sequentially as previously described (Zhao et al., 2016). The isolated mouse OPCs were cultured in the Growth Medium plus B27, 1 ng/ml NT3, and 5 mM forskolin (Emery et al., 2009).

METHOD DETAILS

Tissue Processing, Histology, and Imaging—Mice at various developmental stages were anesthetized with ketamine/xylazine and perfused with PBS followed by 4% paraformaldehyde. Spinal cords or brains were dissected, fixed in 4% paraformaldehyde overnight, cryoprotected in 25% sucrose at 4°C, embedded in OCT and cryosectioned at 16 μm. For immunostaining, we used antibodies to PDGFRα (BD Bioscience, 558774), anti-Olig2 (Millipore, AB9610), CC1 (Calbiochem, OP80), MBP (Santa Cruz, sc-13914), NeuN (Millipore), GFAP (Sigma, G3893), NG2 (Millipore ab5320), Neurofilament M (Millipore, AB1987), CD3 (BioLegend, 100212), Iba1 (Wako, 019-19741) and Lingo1 (Millipore, 07-768), MHCII (BioLegend, 107606), Ly6G (BioLegend, 127606), CD19 (BioLegend, 101504). The fluorescence images in the corresponding CNS regions between control and mutants were acquired under a Nikon E-C2 confocal microscope and quantified in a double-blinded manner by ImageJ. Images from at least five sections per animal were collected for analysis. For immunoblotting, whole cell lysates were prepared in RIPA buffer (ThermoFisher Scientific; cat# 89900) supplemented with a protease inhibitor cocktail (1:200, Sigma-P1860). After western blotting, proteins were detected with appropriate secondary antibodies by using chemiluminescence with the ECL kit (Pierce) according to manufacturer's instructions. For electron microscopy, spinal cord and optic nerves were dissected and fixed in 2.5 % glutaraldehyde and 4% paraformaldehyde in 0.1 M cacodylate buffer (pH 7.2) for 24 hr and processed as previously described (Xin et al., 2005). RNA in situ hybridization was performed using digoxigenin-labeled *PDGFRα, Plp1/Dm-20*, and *Mbp* riboprobes as described previously (Zhao et al., 2010).

siRNA Transfection—siRNA transfection in primary OPCs were carried out by Lipofectamine RNAiMAX (Invitrogen). siRNAs were purchased from Sigma-Aldrich with the following catalogue numbers: control siRNA: MISSION siRNA Universal Negative Control #1 SIC001; mouse *Lingo1* siRNA, SASI_Mm01_00137609; Mouse *Etv5* siRNA, SASI_Mm01_00026515, rat *Lingo1* siRNA, SASI_Rn02_00324112; rat *Etv5* siRNA, SASI_Rn02_00225316. Rat OPCs were transfected with expression vectors, pCIG, pCIG-Nfib and pCIG-Etv5, by using Nucleofector (Lonza) according to manufacturer's protocol. OPCs were transfected with expressing vectors using Amaxa electroporator according to the manufacturer's protocol and assayed for immunocytochemistry and qRT-PCR analysis.

RNA Extraction and qRT-PCR—Total RNAs were purified from tissues or cell cultures using TRIzol reagent (Invitrogen) according to the manufacturer's instructions. RNA was transcribed to cDNA with the First-Strand cDNA Synthesis Kit (Bio-rad, Cat # 170-8890). Quantitative real-time PCR was performed using the ABI Prism 7700 Sequence Detector System (Perkin-Elmer Applied Biosystems), and the relative gene expression was normalized to an internal control such as *Gapdh* or *U6*. Stem-loop RT-PCR was used for the

quantification of mature miR-219 expression levels as described previously (Zhao et al., 2010).

Luciferase Reporter Assays—miR-219 locus on chromosome 2 with their ~200 bp flanking sequences were amplified by PCR from mouse genomic DNA and inserted into pCIG vector (Zhao et al., 2010). Segments carrying putative *miR-219* binding sites in 3 coding regions and 3′ UTRof *Nfia, Nfib, Etv5* and *Lingo1* were cloned into pMIR-REPORT vector (Ambion, AM5795) as described previously (Zhao et al., 2010). For mutagenesis of *miR-219* binding sites, two predicted binding sites in pMir-reporter-*Nfia* UTR, pMir-reporter-*Nfib* CD, pMir-reporter-*Etv5* CD&UTR, and two predicted binding sites in pMir-reporter-*Lingo1* UTR from “ACAATC” to “CTGCAG” respectively, were created by using GenEdit Site-Directed DNA Mutagenesis Kit (FirstBiotech Cat # 201321). Luciferase reporter constructs were co-transfected with vectors expressing *miR-219* into 293T cells by PolyJet. The pCMV-LacZ plasmid was included as a control for transfection efficiencies. Luciferase activity was assayed 48 hr after transfection using the bright-Glo reporter assay system (Promega, E2610) and FluoReporter lacZ/Galactosidase Quantitation Kit (Life Technologies, F-2905).

LPC-Induced Demyelinating Lesions—6- to 8-week-old *miR-219-1*$^{lox/lox}$, *miR-219-2*$^{lox/lox}$, *Rosa2*^{tdTomato}, *Plp-CreERt* mice and *miR-219-1*$^{lox/+}$, *miR-219-2*$^{lox/+}$, *Rosa2*^{tdTomato}, *Plp-CreERt* control mice, wild type and *miR-219* transgenic mice were used in the lysolecithin-induced demyelination experiments. Anesthesia was induced and maintained by i.p. injection of a mixture of ketamine (90 mg/kg) and xylazine (10 mg/kg). After exposing the spinal vertebrae at the level of T9-T12, meningeal tissue in the intervertebral space was cleared, and the dura was pierced with a dental needle. 0.5 μl of 1 % lysolecithin (*l*-α-lysophosphatidylcholine, Sigma L4129) via a Hamilton syringe attached a glass micropipette was injected into the ventrolateral white matter using a stereotactic apparatus. LPC-induced lesions in brain were stereotactically performed to the genu of corpus callosum. Injuries were conducted in a genotype-blinded manner. For tamoxifen treatment of *Plp-CreERt-miR-219-1/2*$^{lox/lox}$ mice, tamoxifen (Sigma T5648) was dissolved in corn oil (Sigma, C-8267) and injected intraperitoneally at 50 mg/kg body weight (Sigma). Tissues carrying the lesions were collected at different time points.

miRNA Mimic Administration—miRVana miRNA Mimic Negative Control or miR-219 mimic (100 μM; Life Technologies) was mixed with the transfection reagent, i-Fect (Neuromics, NI35150), which allows efficient delivery of miRNAs in vivo, in a ratio of 1:5 (w:v), containing 1% lysolecithin and injected into the ventral white matter of 6- to 8-wk-old wild-type mice. Control or miR-219 mimic with i-Fect mix (10 μl each mouse) were delivered to the lumbar region of the spinal cord via the intrathecal catheters essentially as previously described (Njoo et al., 2014). Injections were performed daily after spinal cord injury until the mice were euthanized for tissue harvest. For intranasal delivery of miRNA mimic, mice were intranasally administered with control and miR-219 mimics. 14 μl of control and miR-219 mimics were administered over a 20 min period at a rate of 2 ml per minute to alternating nostrils. 8 days later, animals were harvested, their brains were sectioned and processed for histology and immunohistochemistry.

Biotin-miRNA Pull-Down Assays—Rat OPCs were transfected with biotin-tagged miR-219 mimics or control cel-miR-67 (Dharmacon) at a final concentration of 40 nM using Lipofectamine 2000 (Life Tech). Forty-eight hours later, the cells were lysed in lysis buffer [20 mM Tris pH 7.5, 200 mM NaCl, 2.5 mM $MgCl_2$, 0.05% Igepal, 60 U Superase-In/ml (Ambion, AM2694), 1 mM DTT, 1 × Pefabloc (Sigma)]. The streptavidin-agarose beads (GE Healthcare, 17-5113-01) were incubated with cell lysate at 4 °C for 1 hour followed by washing with lysis buffer. Total mRNAs bound to the streptavidin beads were extracted by using TRIzol LS (Invitrogen). The pull-down mRNA level was quantified by mRNA-seq. The total mRNA from OPC transfected with biotin-tagged miR-219 mimics or control cel-miR-67 (Dharmacon) as input was quantified by mRNA-seq. The enrichment ratio was calculated, [miR-219/Ctrl (Pulldown)]/[miR-219/Ctrl (Input)] (Lal et al., 2011).

RNA-seq and Data Analysis—The RNA isolated from the optic nerves of P12 control and *miR-219*-dCKO mice, the RNA from rat OPC culture transfected with control miRNA and miR-219 mimic, and the RNA from biotin-tagged miR-219 mimics or control cel-miR-67 pull down assays subject to mRNA deep sequencing. RNA-seq libraries were prepared using the Illumina RNA-Seq Preparation Kit and sequenced by a HiSeq 2000 sequencer (Illumina). All RNA-Seq data from mouse samples were aligned to mm9 and data from rat samples were aligned to Rn4 using TopHat with default settings (http://tophat.cbcb.umd.edu). TopHat output data were analyzed by Cufflinks to estimate FPKM values for known transcripts and to analyze differentially expressed transcripts. A heatmap of gene expression was generated using R language (http://www.r-project.org). GO-analysis of genes repressed in miR-219 mimic transfected OPC and differentiating OL was performed using Toppfun (https://toppgene.cchmc.org/enrichment.jsp).

EAE Immunization and Histological Assessment—8-week-old female C57BL/6 (Charles River lab) mice received injections of 200 μg of myelin oligodendrocyte glycoprotein (MOG) 35–55 peptide emulsified in complete Freund's adjuvant (BD Biosciences), supplemented with 600 μg of *Mycobacterium tuberculosis* (strain H37Ra; BD Biosciences). 24 and 72 hour after immunization, mice were given two intraperitoneal injections of 400 ng of pertussis toxins (List Biological Laboratories, Cat#NC9675592). EAE onset was monitored daily and scored with Clinical scores (0 =healthy; 1=flaccid tail; 2 = ataxia and/or paresis of hindlimbs; 3 = paralysis of hindlimbs and/or paresis of forelimbs; 4 = tetraparalysis; 5 = moribund or death). Once disease symptoms peaked (day 19; clinical score ~3) they were randomized into 2 treatment groups, control microRNA mimic and miR-219 mimic was delivered to the lumbar region of the spinal cord via intrathecal administration daily for 5 days. Animals were scored daily while experimenters were blinded to the identity of the treatments, and a two-tailed Student's *t* test was used to compare each treatment.

Histological assessment of lesioned spinal cords was performed as previously described (Lin et al., 2013). Briefly, serial cross-sections along the length of the spinal cord from the lumbar 2 to lumbar 4 segment in EAE mice were cut at 16 μm and used for lesion volume and cell density measurement and calculation. Every 10th section in the series was stained with appropriate antibodies or labeled with in situ probes. The immunopositive or labeled

cells within the anterior funiculus medially next to the anterior median fissure in the lumbar spinal cord in each section were measured and counted by NIH Image J software (http://rsb.info.nih.gov/ij/). Cell density in the lesions from the serial sections of each spinal cord was calculated and confined to a volume of 0.001 mm^3. The average percentage of demyelinated area without MBP immunofluorescence over the total white matter area in the lumbar spinal cord in every section was measured by Image J and calculated for statistical analysis. The quantitative analyses were performed in a blinded manner to the experimental groups.

QUANTIFICATION AND STATISTICAL ANALYSIS

All data analyses were done using GraphPad Prism 6.00 (San Diego, California, www.graphpad.com). Data are shown as mean ± S.E.M. Animals of the same genotype and age exhibited very similar phenotypes. Littermate controls minimized any difference imparted by background. Quantifications were performed from at least three independent experiments and quantified blindly. Tests assumed a normal distribution. For cell-based and gene expression assays as well as phenotypic analysis, no statistical methods were used to predetermine sample sizes, but our sample sizes are similar to those generally employed in the field. For the miR-219 treatment study in mice, animal groups were randomized during treatment. Statistical significance was determined using unpaired Student's *t* test between two groups. One-way ANOVA was performed with multiple comparisons or pairwise comparisons following Tukey's ranking tests when comparing multiple groups. $p < 0.05$ is considered to be statistically significant.

DATA AND SOFTWARE AVAILABILITY

All the RNA-seq data have been deposited in the NCBI Gene Expression Omnibus (GEO) under accession number GEO: GSE80439.

Supplementary Material

Refer to Web version on PubMed Central for supplementary material.

Acknowledgments

The authors would like to thank Bradley Meyer and Xianyao Zhou for technical support and graphic images and Dr. Thomas Carroll for Par3 floxed mice. We thank Dr. Olga Barca and Dr. Edward Hurlock for suggestions. This study was funded in part by grants from the US NIH (R01NS072427 and R01NS075243) to Q.R.L., the National Multiple Sclerosis Society (NMSS-4727) to Q.R.L., and NIH (R01NS065808 and R21NS087474) and National Multiple Sclerosis Society grant RG 4172-A-4 to E.R.B.

References

Alexiou P, Maragkakis M, Papadopoulos GL, Reczko M, Hatzigeorgiou AG. Lostin translation: anassessment and perspective for computational microRNA target identification. Bioinformatics. 2009; 25:3049–3055. [PubMed: 19789267]

Bartel DP. MicroRNAs: target recognition and regulatory functions. Cell. 2009; 136:215–233. [PubMed: 19167326]

Bittner, S., Afzali, AM., Wiendl, H., Meuth, SG. Myelin oligodendrocyte glycoprotein (MOG3555) induced experimental autoimmune encephalomyelitis (EAE) in C57BL/6 mice. J Vis Exp. 2014. http://dx.doi.org/10.3791/51275

Bruck W. The pathology of multiple sclerosis is the result of focal inflammatory demyelination with axonal damage. J Neurol. 2005; 252(Suppl 5):v3–v9. [PubMed: 16254699]

Castelli M, Boca M, Chiaravalli M, Ramalingam H, Rowe I, Distefano G, Carroll T, Boletta A. Polycystin-1 binds Par3/aPKC and controls convergent extension during renal tubular morphogenesis. Nat Commun. 2013; 4:2658. [PubMed: 24153433]

Chang A, Tourtellotte WW, Rudick R, Trapp BD. Premyelinating oligodendrocytes in chronic lesions of multiple sclerosis. N Engl J Med. 2002; 346:165–173. [PubMed: 11796850]

Cho WC. MicroRNAs as therapeutic targets and their potential applications in cancer therapy. Expert Opin Ther Targets. 2012; 16:747–759. [PubMed: 22690697]

Deneen B, Ho R, Lukaszewicz A, Hochstim CJ, Gronostajski RM, Anderson DJ. The transcription factor NFIA controls the onset of gliogenesis in the developing spinal cord. Neuron. 2006; 52:953–968. [PubMed: 17178400]

Deshmukh VA, Tardif V, Lyssiotis CA, Green CC, Kerman B, Kim HJ, Padmanabhan K, Swoboda JG, Ahmad I, Kondo T, et al. A regenerative approach to the treatment of multiple sclerosis. Nature. 2013; 502:327–332. [PubMed: 24107995]

Doerflinger NH, Macklin WB, Popko B. Inducible site-specific recombination in myelinating cells. Genesis. 2003; 35:63–72. [PubMed: 12481300]

Dugas JC, Cuellar TL, Scholze A, Ason B, Ibrahim A, Emery B, Zamanian JL, Foo LC, McManus MT, Barres BA. Dicer1 and miR-219 are required for normal oligodendrocyte differentiation and myelination. Neuron. 2010; 65:597–611. [PubMed: 20223197]

Emery B, Agalliu D, Cahoy JD, Watkins TA, Dugas JC, Mulinyawe SB, Ibrahim A, Ligon KL, Rowitch DH, Barres BA. Myelin gene regulatory factor is a critical transcriptional regulator required for CNS myelination. Cell. 2009; 138:172–185. [PubMed: 19596243]

Fancy SP, Baranzini SE, Zhao C, Yuk DI, Irvine KA, Kaing S, Sanai N, Franklin RJ, Rowitch DH. Dysregulation of the Wnt pathway inhibits timely myelination and remyelination in the mammalian CNS. Genes Dev. 2009; 23:1571–1585. [PubMed: 19515974]

Fancy SP, Glasgow SM, Finley M, Rowitch DH, Deneen B. Evidence that nuclear factor IA inhibits repair after white matter injury. Ann Neurol. 2012; 72:224–233. [PubMed: 22807310]

Franklin RJ. Why does remyelination fail in multiple sclerosis? Nat Rev Neurosci. 2002; 3:705–714. [PubMed: 12209119]

Franklin RJ, Gallo V. The translational biology of remyelination: past, present, and future. Glia. 2014; 62:1905–1915. [PubMed: 24446279]

Gallo V, Deneen B. Glial development: the crossroads of regeneration and repair in the CNS. Neuron. 2014; 83:283–308. [PubMed: 25033178]

Glasgow SM, Zhu W, Stolt CC, Huang TW, Chen F, LoTurco JJ, Neul JL, Wegner M, Mohila C, Deneen B. Mutual antagonism between Sox10 and NFIA regulates diversification of glial lineages and glioma subtypes. Nat Neurosci. 2014; 17:1322–1329. [PubMed: 25151262]

Gravel M, Di Polo A, Valera PB, Braun PE. Four-kilobase sequence of the mouse CNP gene directs spatial and temporal expression of lacZ in transgenic mice. J Neurosci Res. 1998; 53:393–404. [PubMed: 9710259]

Grimson A, Farh KK, Johnston WK, Garrett-Engele P, Lim LP, Bartel DP. MicroRNA targeting specificity in mammals: determinants beyond seed pairing. Mol Cell. 2007; 27:91–105. [PubMed: 17612493]

Guo H, Ingolia NT, Weissman JS, Bartel DP. Mammalian microRNAs predominantly act to decrease target mRNA levels. Nature. 2010; 466:835–840. [PubMed: 20703300]

He X, Yu Y, Awatramani R, Lu QR. Unwrapping myelination by MicroRNAs. Neuroscientist. 2012; 18:45–55. [PubMed: 21536841]

Hudish LI, Blasky AJ, Appel B. miR-219 regulates neural precursor differentiation by direct inhibition of apical par polarity proteins. Dev Cell. 2013; 27:387–398. [PubMed: 24239515]

Inui M, Martello G, Piccolo S. MicroRNA control of signal transduction. Nat Rev Mol Cell Biol. 2010; 11:252–263. [PubMed: 20216554]

Junker A, Hohlfeld R, Meinl E. The emerging role of microRNAs in multiple sclerosis. Nat Rev Neurol. 2011; 7:56–59. [PubMed: 21151203]

Kiyota T, Kato A, Kato Y. Ets-1 regulates radial glia formation during vertebrate embryogenesis. Organogenesis. 2007; 3:93–101. [PubMed: 19279707]

Klaes A, Menne T, Stollewerk A, Scholz H, Klambt C. The Ets transcription factors encoded by the *Drosophila* gene pointed direct glial cell differentiation in the embryonic CNS. Cell. 1994; 78:149–160. [PubMed: 8033206]

Krek A, Grun D, Poy MN, Wolf R, Rosenberg L, Epstein EJ, MacMenamin P, da Piedade I, Gunsalus KC, Stoffel M, et al. Combinatorial microRNA target predictions. Nat Genet. 2005; 37:495–500. [PubMed: 15806104]

Kuhlmann T, Miron V, Cui Q, Wegner C, Antel J, Bruck W. Differentiation block of oligodendroglial progenitor cells as a cause for remyelination failure in chronic multiple sclerosis. Brain. 2008; 131:1749–1758. [PubMed: 18515322]

Lal A, Thomas MP, Altschuler G, Navarro F, O'Day E, Li XL, Concepcion C, Han YC, Thiery J, Rajani DK, et al. Capture of microRNA-bound mRNAs identifies the tumor suppressor miR-34a as a regulator of growth factor signaling. PLoS Genet. 2011; 7:e1002363. [PubMed: 22102825]

Lau P, Verrier JD, Nielsen JA, Johnson KR, Notterpek L, Hudson LD. Identification of dynamically regulated microRNA and mRNA networks in developing oligodendrocytes. J Neurosci. 2008; 28:11720–11730. [PubMed: 18987208]

Leung AK, Sharp PA. MicroRNA functions in stress responses. Mol Cell. 2010; 40:205–215. [PubMed: 20965416]

Li X, Newbern JM, Wu Y, Morgan-Smith M, Zhong J, Charron J, Snider WD. MEK is a key regulator of gliogenesis in the developing brain. Neuron. 2012; 75:1035–1050. [PubMed: 22998872]

Lin ST, Fu YH. miR-23 regulation of lamin B1 is crucial for oligodendrocyte development and myelination. Dis Model Mech. 2009; 2:178–188. [PubMed: 19259393]

Lin W, Lin Y, Li J, Fenstermaker AG, Way SW, Clayton B, Jamison S, Harding HP, Ron D, Popko B. Oligodendrocyte-specific activation of PERK signaling protects mice against experimental autoimmune encephalomyelitis. J Neurosci. 2013; 33:5980–5991. [PubMed: 23554479]

Mendell JT, Olson EN. MicroRNAs in stress signaling and human disease. Cell. 2012; 148:1172–1187. [PubMed: 22424228]

Mi S, Hu B, Hahm K, Luo Y, Kam Hui ES, Yuan Q, Wong WM, Wang L, Su H, Chu TH, et al. LINGO-1 antagonist promotes spinal cord remyelination and axonal integrity in MOG-induced experimental autoimmune encephalomyelitis. Nat Med. 2007; 13:1228–1233. [PubMed: 17906634]

Miska EA, Alvarez-Saavedra E, Abbott AL, Lau NC, Hellman AB, McGonagle SM, Bartel DP, Ambros VR, Horvitz HR. Most *Caenorhabditis elegans* microRNAs are individually not essential for development or viability. PLoS Genet. 2007; 3:e215. [PubMed: 18085825]

Njoo, C., Heinl, C., Kuner, R. In vivo SiRNA transfection and gene knockdown in spinal cord via rapid noninvasive lumbar intrathecal injections in mice. J Vis Exp. 2014. http://dx.doi.org/10.3791/51229

Orom UA, Lund AH. Isolation of microRNA targets using biotinylated synthetic microRNAs. Methods. 2007; 43:162–165. [PubMed: 17889804]

Pusic AD, Kraig RP. Youth and environmental enrichment generate serum exosomes containing miR-219 that promote CNS myelination. Glia. 2014; 62:284–299. [PubMed: 24339157]

Rehmsmeier M, Steffen P, Hochsmann M, Giegerich R. Fast and effective prediction of microRNA/target duplexes. RNA. 2004; 10:1507–1517. [PubMed: 15383676]

Rigoutsos I. New tricks for animal microRNAs: targeting of amino acid coding regions at conserved and nonconserved sites. Cancer Res. 2009; 69:3245–3248. [PubMed: 19351814]

Sabo JK, Aumann TD, Merlo D, Kilpatrick TJ, Cate HS. Remyelination is altered by bone morphogenic protein signaling in demyelinated lesions. J Neurosci. 2011; 31:4504–4510. [PubMed: 21430151]

Sakai K, Miyazaki J. A transgenic mouse line that retains Cre recombinase activity in mature oocytes irrespective of the cre transgene transmission. Biochem Biophys Res Commun. 1997; 237:318–324. [PubMed: 9268708]

Shin D, Shin JY, McManus MT, Ptacek LJ, Fu YH. Dicer ablation in oligodendrocytes provokes neuronal impairment in mice. Ann Neurol. 2009; 66:843–857. [PubMed: 20035504]

Stefani G, Slack FJ. Small non-coding RNAs in animal development. Nat Rev Mol Cell Biol. 2008; 9:219–230. [PubMed: 18270516]

Vicente R, Noel D, Pers YM, Apparailly F, Jorgensen C. Deregulation and therapeutic potential of microRNAs in arthritic diseases. Nat Rev Rheumatol. 2016; 12:496.

Wolswijk G. Chronic stage multiple sclerosis lesions contain a relatively quiescent population of oligodendrocyte precursor cells. J Neurosci. 1998; 18:601–609. [PubMed: 9425002]

Xin M, Yue T, Ma Z, Wu FF, Gow A, Lu QR. Myelinogenesis and axonal recognition by oligodendrocytes in brain are uncoupled in Olig1-null mice. J Neurosci. 2005; 25:1354–1365. [PubMed: 15703389]

Xin H, Li Y, Buller B, Katakowski M, Zhang Y, Wang X, Shang X, Zhang ZG, Chopp M. Exosome-mediated transfer of miR-133b from multipotent mesenchymal stromal cells to neural cells contributes to neurite outgrowth. Stem Cells. 2012; 30:1556–1564. [PubMed: 22605481]

Ye F, Chen Y, Hoang T, Montgomery RL, Zhao XH, Bu H, Hu T, Taketo MM, van Es JH, Clevers H, et al. HDAC1 and HDAC2 regulate oligodendrocyte differentiation by disrupting the beta-catenin-TCF interaction. Nat Neurosci. 2009; 12:829–838. [PubMed: 19503085]

Zhang Y, Argaw AT, Gurfein BT, Zameer A, Snyder BJ, Ge C, Lu QR, Rowitch DH, Raine CS, Brosnan CF, et al. Notch1 signaling plays a role in regulating precursor differentiation during CNS remyelination. Proc Natl Acad Sci USA. 2009; 106:19162–19167. [PubMed: 19855010]

Zhao X, He X, Han X, Yu Y, Ye F, Chen Y, Hoang T, Xu X, Mi QS, Xin M, et al. MicroRNA-mediated control of oligodendrocyte differentiation. Neuron. 2010; 65:612–626. [PubMed: 20223198]

Zhao C, Deng Y, Liu L, Yu K, Zhang L, Wang H, He X, Wang J, Lu C, Wu LN, et al. Dual regulatory switch through interactions of Tcf7l2/Tcf4 with stage-specific partners propels oligodendroglial maturation. Nat Commun. 2016; 7:10883. [PubMed: 26955760]

In Brief

Wang et al. show that miR-219 collaborates with miR-338 and is required for proper oligodendrocyte differentiation and myelination in the mammalian CNS by targeting a network of stage-specific differentiation inhibitors, including Lingo1 and Etv5. Therapeutic delivery of miR-219 also enhances myelin repair in animal models of multiple sclerosis.

Highlights

- miR-219 is critical for oligodendrocyte differentiation and myelination in murine CNS
- miR-338 deletion exacerbates the dysmyelination phenotype in miR-219-deficient mice
- miR-219 targets stage-specific inhibitors and Lingo1-Etv5 to promote CNS myelination
- miR-219 mimics augment remyelination and functional recovery in demyelinating models

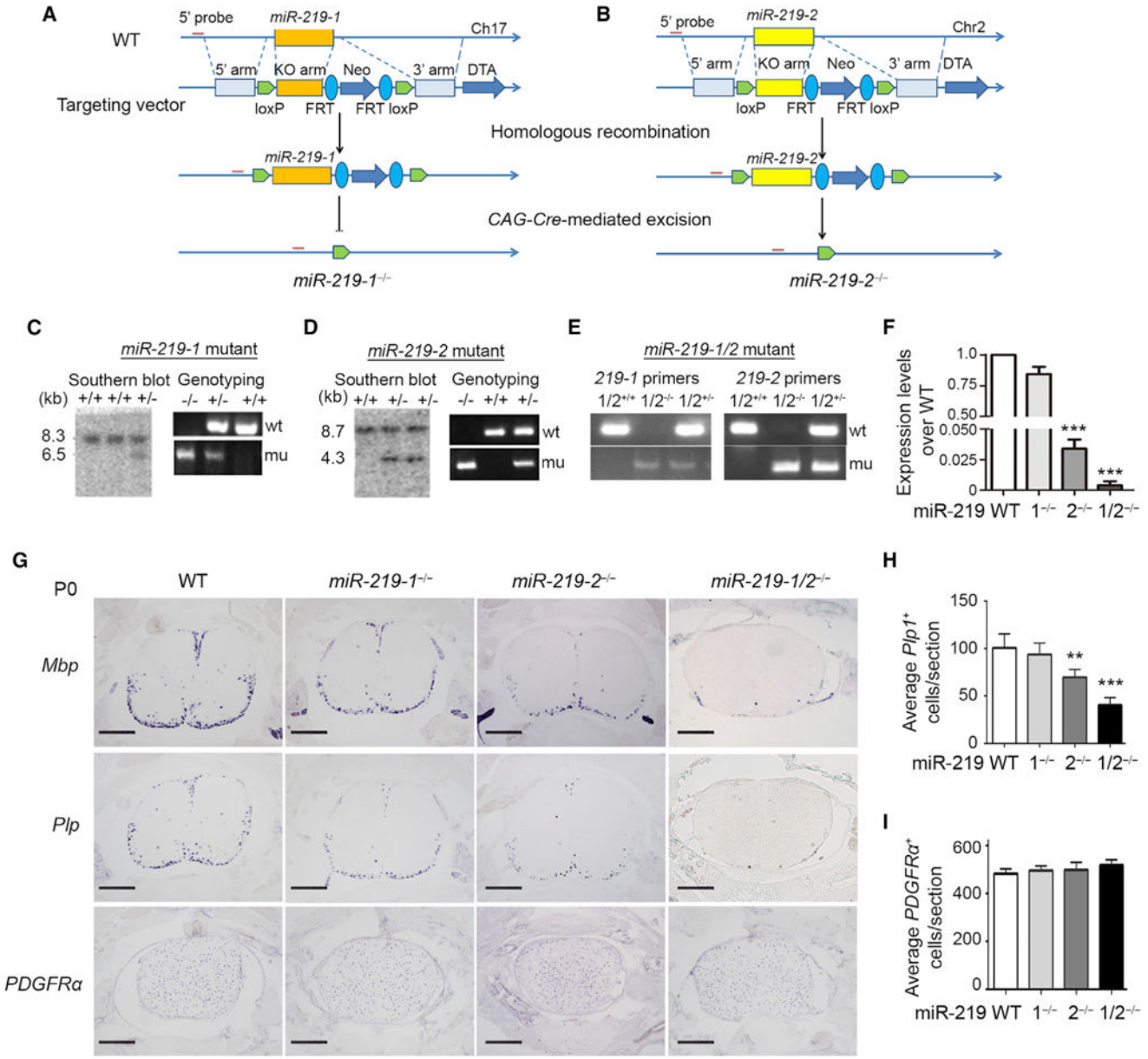

Figure 1. *miR-219*-Null Mice Exhibit Defective Myelination in Spinal Cord

(A and B) Schematic design of (A) *miR-219-1* and (B) *miR-219-2* floxed alleles. Neo, neomycin cassette; Frt, flippase recognition targets; and DTA, the diphtheria toxin gene. The red lines: 5′ external probes for Southern blot.

(C and D) Southern blot (left) and genotyping patterns (right) of (C) *miR-219-1* and (D) *miR-219-2* mutant mice. Embryonic DNAs digested with (C) SacI and (D) NheI were used for Southern blotting to identify the targeted loci as 6.5-kb and 4.3-kb bands for *miR-219-1* or *−2* mutants, respectively.

(E) Genotyping patterns for wild-type (WT), *miR-219-1/2*$^{+/-}$ and *miR-219-1/2*$^{-/-}$.

(F) qRT-PCR analysis of WT, miR-219 in *miR-219* single and double mutant optic nerves at P12. Data are means ±SEM, $n = 3$ animals/genotype. ***$p < 0.001$, one-way ANOVA with Tukey's multiple-comparison test.

(G) RNA in situ hybridization for *Mbp*, *Plp1*, and *PDGFRα* on the spinal cord from wild-type, *miR-219* single and double mutants at P0. Scale bar, 100 μm.
(H and I) Quantification of *Plp1* expressing cells (H), *PDGFRα* expressing cells (I) in the spinal cord of WT, *miR-219* single and double mutants. Data are means ±SEM, $n = 3$ animals/genotype. **$p < 0.01$, ***$p < 0.001$, one-way ANOVA with Tukey's multiple-comparison test.

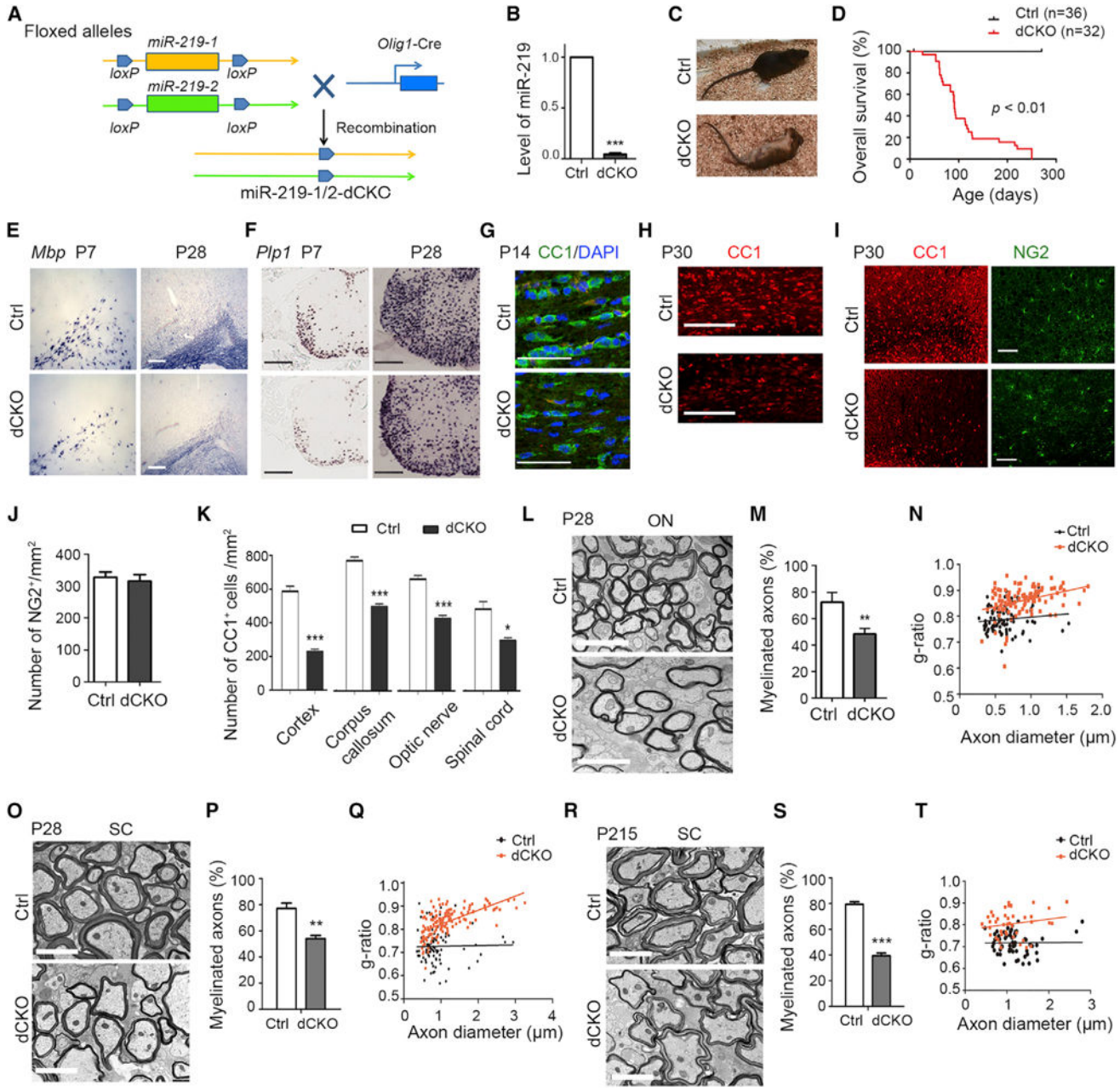

Figure 2. *miR-219* Ablation in Oligodendrocyte Lineage Cells Impairs CNS Myelination

(A) Schematic diagram depicting *Olig1-Cre*-mediated excision of the floxed *miR-219* alleles to generate *miR-219*-dCKO mice.

(B) qRT-PCR analysis of miR-219 in heterozygous control (Ctrl) and *miR-219*-dCKO optic nerves at P12. $n = 3$ animals/genotype.

(C) Photographs of Ctrl and *miR-219*-dCKO mice at P90. The dCKO mouse is suffering from seizure.

(D) Survival curve of Ctrl and miR-219-dCKO mice. $p < 0.01$, Kaplan-Meier curve with log-rank test.

(E and F) RNA in situ hybridization for *Mbp* (E) and *Plp1* (F) in the brain of Ctrl and miR-219-dCKO mice at indicated ages. Scale bars: (E) 100 μm; (F) 200 μm.

(G–I) Immunohistochemistry for CC1 counterstained with DAPI in the optic nerve at P14 (G) and the corpus callosum at P30 (H) and for CC1 and NG2 in the cortices at P30 of Ctrl and *miR-219*-dCKO (H). Scale bars: 50 μm.

(J) $NG2^+$ cells per mm^2 in the cortex of Ctrl and *miR-219*-dCKO mice at P30. $n = 3$ animals/genotype (Student's t test).

(K) $CC1^+$ cells per mm^2 in the cortex and corpus callosum at P30, optic nerve at P14, and spinal cord at P7 of Ctrl and *miR-219*-dCKO mice. $n = 3$ animals/genotype.

(L) EM images of optic nerves from Ctrl and *miR-219*-dCKO mice at P28. Scale bars: 2 μm.

(M and N) The percentage of myelinated axons (M) and myelin *g* ratio (N) of Ctrl and dCKO spinal cords at P28. $n = 3$ animals/genotype. *g*-ratio scatterplot in (N), $p < 0.001$; Student's t test.

(O) EM images of the spinal white matter from Ctrl and *miR-219*-dCKO mice at P28. Scale bars: 2 μm.

(P) The percentage of myelinated axons of Ctrl and dCKO spinal cords at P28. $n = 3$ animals/genotype. $^{**}p < 0.01$, Student's t test.

(Q) Scatterplot of the myelin *g* ratios of Ctrl and *miR-219*-dCKO spinal cords at P28. $n = 3$ animals/genotype. $p < 0.001$, Student's t test.

(R) EM images of the spinal white matter from Ctrl and *miR-219*-dCKO mice at P215. Scale bars: 2 μm.

(S and T) The percentage of myelinated axons (S) and myelin *g* ratio (T) of Ctrl and *miR-219*-dCKO spinal cords at P215.$n = 3$ animals/genotype.*g*-ratio scatterplot in (T), $p < 0.001$; Student's t test.

Data in (B), (J), (M), (P) and (S) are presented as means ±SEM. $^{*}p < 0.05$, $^{**}p < 0.01$, $^{***}p < 0.001$, Student's t test.

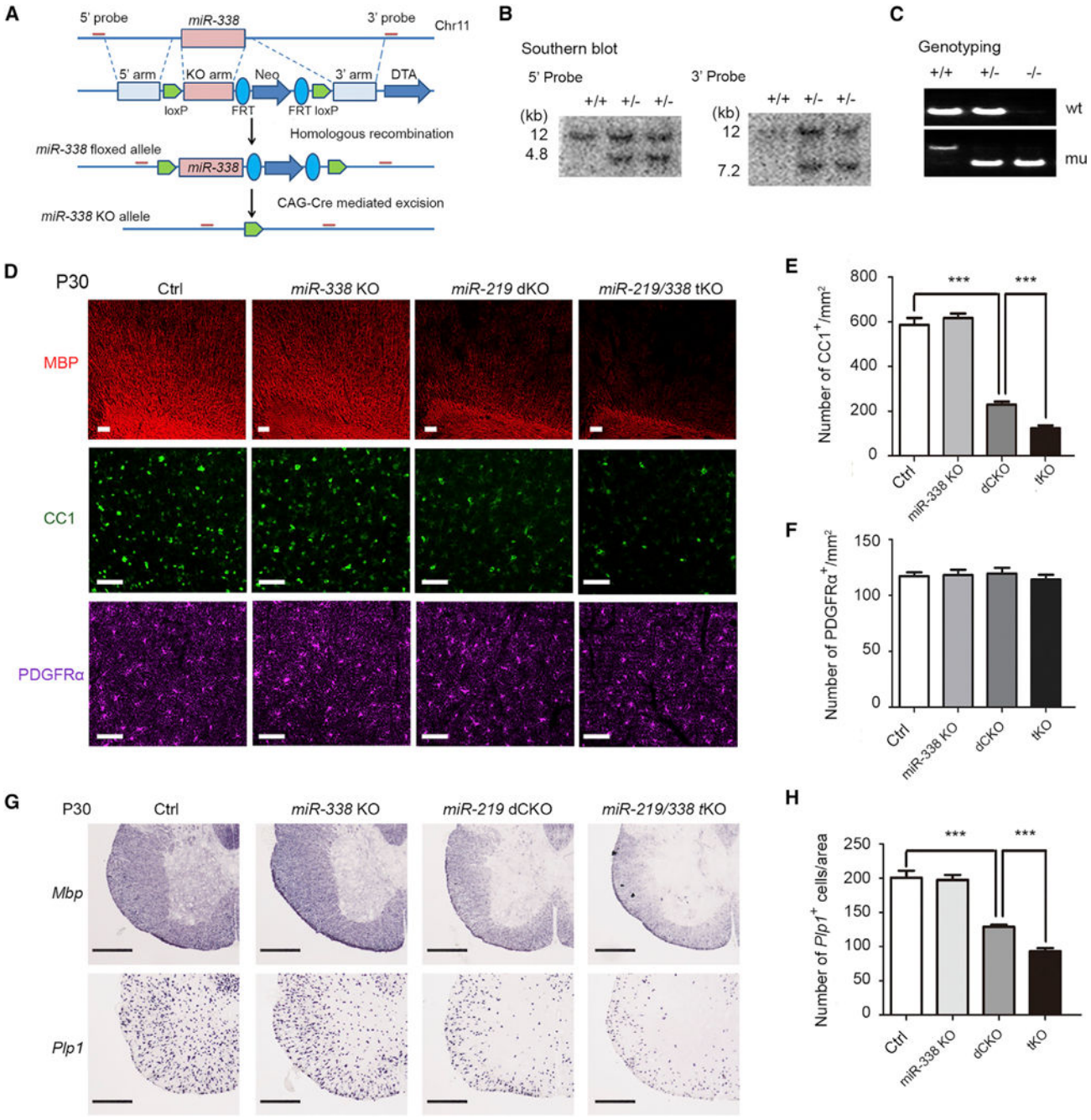

Figure 3. *miR-338* Deletion Aggravates the Dysmyelination Phenotype in *miR-219* Mutants

(A) Schematic design for generating *miR-338* knockout mice. The red lines: 5′ and 3′ external probes for Southern blot.

(B) Southern blot of genomic DNA digested with KpnI with 5′ and 3′ external probes.

(C) Genotyping patterns of *miR-338* heterozygous and null mice.

(D) Immunohistochemistry for MBP, CC1, and PDGFRα in brain sections of Ctrl, *miR-338* KO, *miR-219*-dCKO, and *miR-219/miR-338* tKO mice at P30. Scale bar: 50 μm.

(E and F) Quantification of (E) $CC1^+$ and (F) $PDGFR\alpha^+$ cell density in the cortices from indicated mice.

(G) RNA in situ hybridization for *Mbp* and *Plp* on spinal cord sections from indicated mice at P30. Scale bar: 200 μm.

(H) Average number of *Plp1*$^{+}$ cells per area (0.2 mm^{2}) at the posterior funiculus from indicated mice.

Data in (E), (F), and (H) are presented as means ±SEM, n = 3 animals/genotype. ***p < 0.001, one-way ANOVA with Tukey's multiple-comparison test.

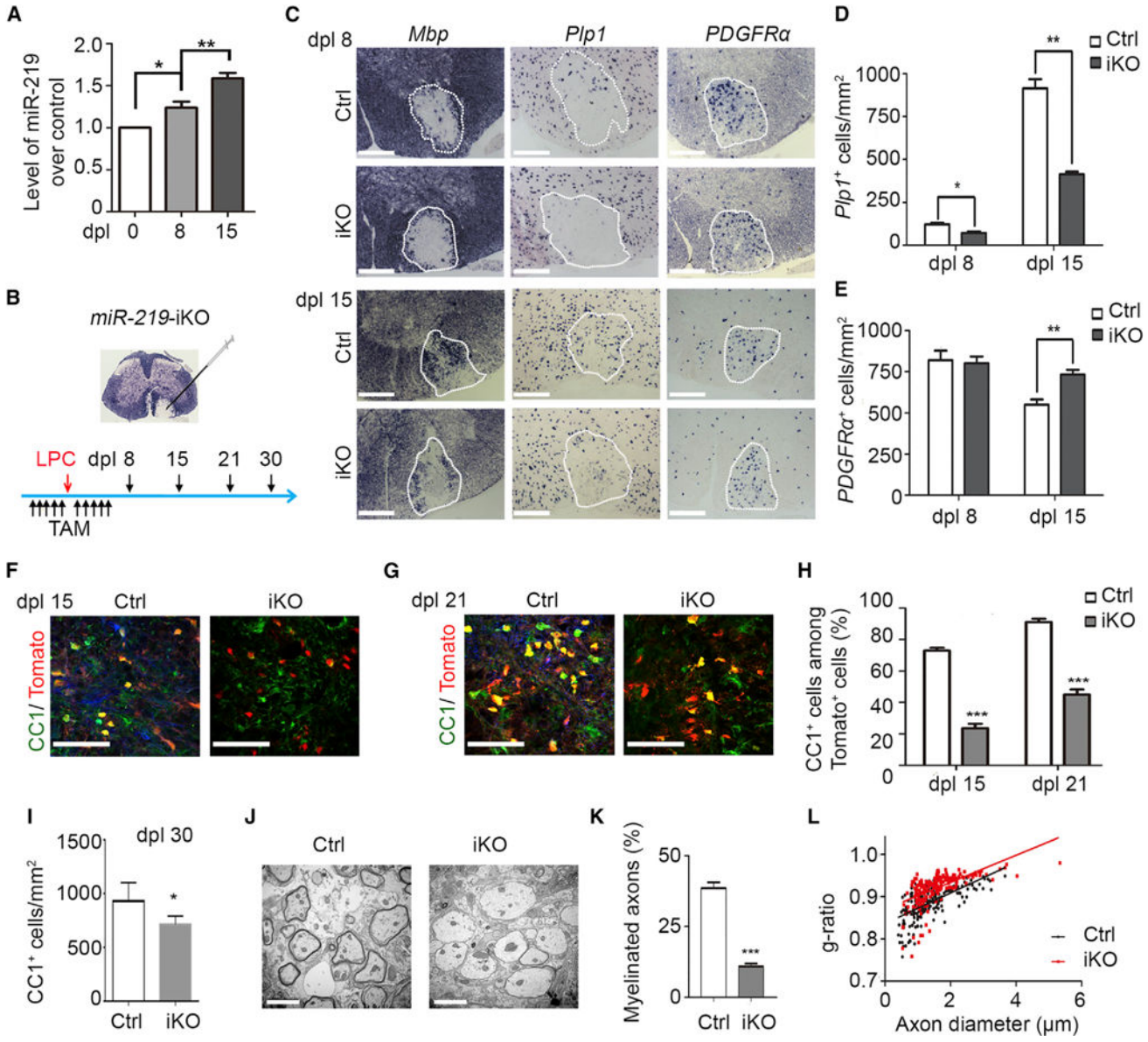

Figure 4. *miR-219* Ablation Impairs Remyelination in an LPC Injury Mouse Model

(A) qRT-PCR analysis of miR-219 levels in spinal lesion tissues over vehicle-injected control at dpl 0, 8, and 15. Data are means ±SEM, $n = 4$ animals/stage. *p < 0.05, **p < 0.01, one-way ANOVA with Tukey's multiple-comparison test.

(B) Tamoxifen (TAM)-induced *miR-219* deletion and LPC-induced demyelination in the spinal cord of *miR-219-iKO* (iKO) mice.

(C) RNA in situ hybridization for *Mbp, Plp1*, and *PDGFRα* in the LPC lesions (dashed circle) of Ctrl and iKO at dpl 8 and 15. Scale bars: 100 μm.

(D and E) Quantification of (D) $Plp1^+$ and (E) $PDGFR\alpha^+$ cells per mm^2 in the LPC lesions of Ctrl and iKO mice at dpl 8 and 15. Data are means ±SEM, at dpl 8, $n = 6$ Ctrl and 7 iKO mice; at dpl 15, $n = 7$ Ctrl and 8 iKO mice. *p < 0.05, **p < 0.01, Student's t test.

(F and G) Immunostaining for CC1 in the LPC lesions of Ctrl and iKO mice at (F) dpl 15 and (G) dpl 21. Expression of tdTomato (red) indicates cells with miR-219 deletion. Scale bars: 100 μm.

(H) Percentage of tdTomato cells that were $CC1^+$ in LPC lesions in Ctrl and iKO mice at dpl 15and 21. Data are means ±SEM, $n = 6$ animals/genotype. ***$p < 0.001$, Student's t test.

(I) $CC1^+$ cell density in LPC lesion areas in Ctrl and iKO mice at dpl 30. Data are means ±SEM, $n = 6$ animals/genotype. *$p < 0.05$, Student's t test.

(J) EM of LPC lesions in the ventral spinal cords from Ctrl and iKO mice at dpl 15. Scale bars: 2 μm.

(K) The percentage of remyelinated axons in LPC lesions of Ctrl and iKO mice at dpl 15. Data are means ±SEM, $n = 4$ animals/genotype. ***$p < 0.001$, Student's t test.

(L) The plot of *g* ratio versus axon diameter in LPC lesions of Ctrl (black) and iKO (red) mice at dpl 15. $n = 4$ animals/genotype. $p < 0.001$, Student's t test.

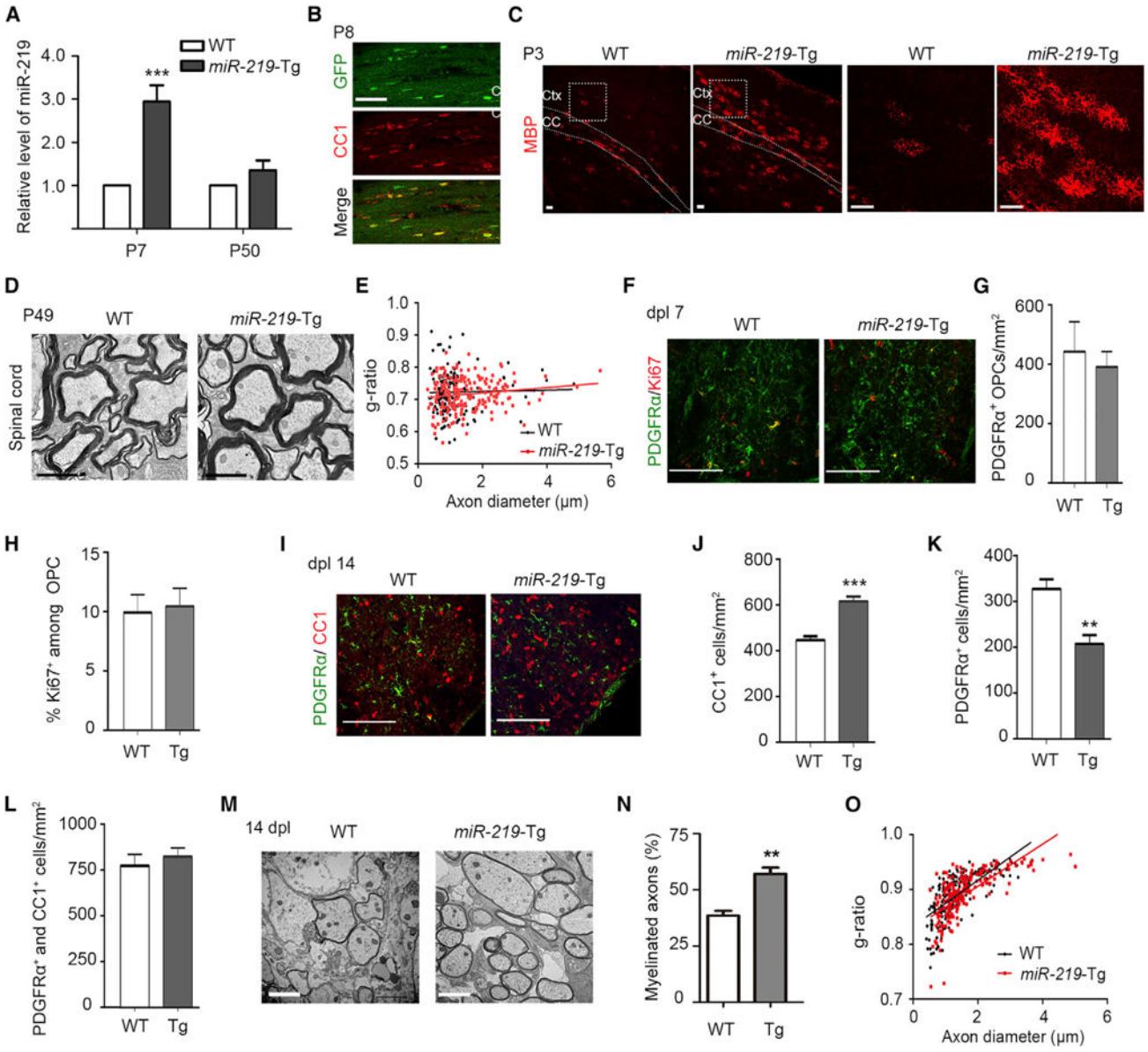

Figure 5. Remyelination Is Enhanced in *miR-219* Transgenic Mice

(A) qRT-PCR analysis of miR-219 in the corpus callosum from wild-type (WT) and *miR-219*-Tg mice atP7 and P50.n = 3animals/genotype. ***p < 0.001, Student's t test.

(B) Expression of GFP and CC1 in the corpus callosum (CC) of *miR-219*-Tg mice at P8. Scale bar: 100 μm.

(C) Immunostaining of MBP in the cortices of WT and *miR-219*-Tg mice at P3, and higher magnification of the framed region is shown on the right. Scale bars: 50 μm.

(D) EM images of the ventral spinal white matter from WT and *miR-219*-Tg mice at P49. Scale bars: 2 μm.

(E) The scatterplot of g ratio versus axon diameter at spinal cords of WT and *miR-219*-Tg mice at dpl 14. n = 4 animals/genotype; Student's t test.

(F) Immunostaining for Ki67 and PDGFRα in the LPC lesions of WT and *miR-219*-Tg mice at dpl 7. Scale bars: 100 μm.

(G and H) Quantification of PDGFRα$^+$ OPCs (G) and the percentage Ki67+ cells among PDGFRα$^+$ OPCs (H) in the LPC lesions of WT and*miR-219*-Tg mice at dpl 7. n = 5 animals/genotype; Student's t test.

(I) Immunostaining for CC1 and PDGFRα in the LPC lesions of WT and *miR-219*-Tg mice at dpl 14. Scale bars: 100 μm.

(J–L) Quantification of CC1$^+$ OLs (J), PDGFRα$^+$ OPCs (K), and total of CC1$^+$ OLs plus PDGFRα$^+$ OPCs (L) in the LPC lesions of WT and *miR-219*-Tg mice at dpl 14. n = 6 WT and 8 *miR-219*-Tg mice. **p < 0.01, ***p < 0.001, Student's t test.

(M) EM images of the LPC lesions in the ventral spinal white matter from WT and *miR-219*-Tg mice at dpl 14. Scale bars: 2 μm.

(N) The percentage of remyelinated axons in LPC lesions in the ventral spinal white matter from WT and *miR-219*-Tg mice at dpl 14. n = 4 animals/genotype. **p < 0.01, Student's t test.

(O) The scatterplot of *g* ratio versus axon diameter in LPC-induced lesions of WT and *miR-219*-Tg mice at dpl 14.n=4 animals/genotype. p <0.001, Student's t test.

Data in (A), (G), (H), (J–L), and (N) are presented as means ± SEM.

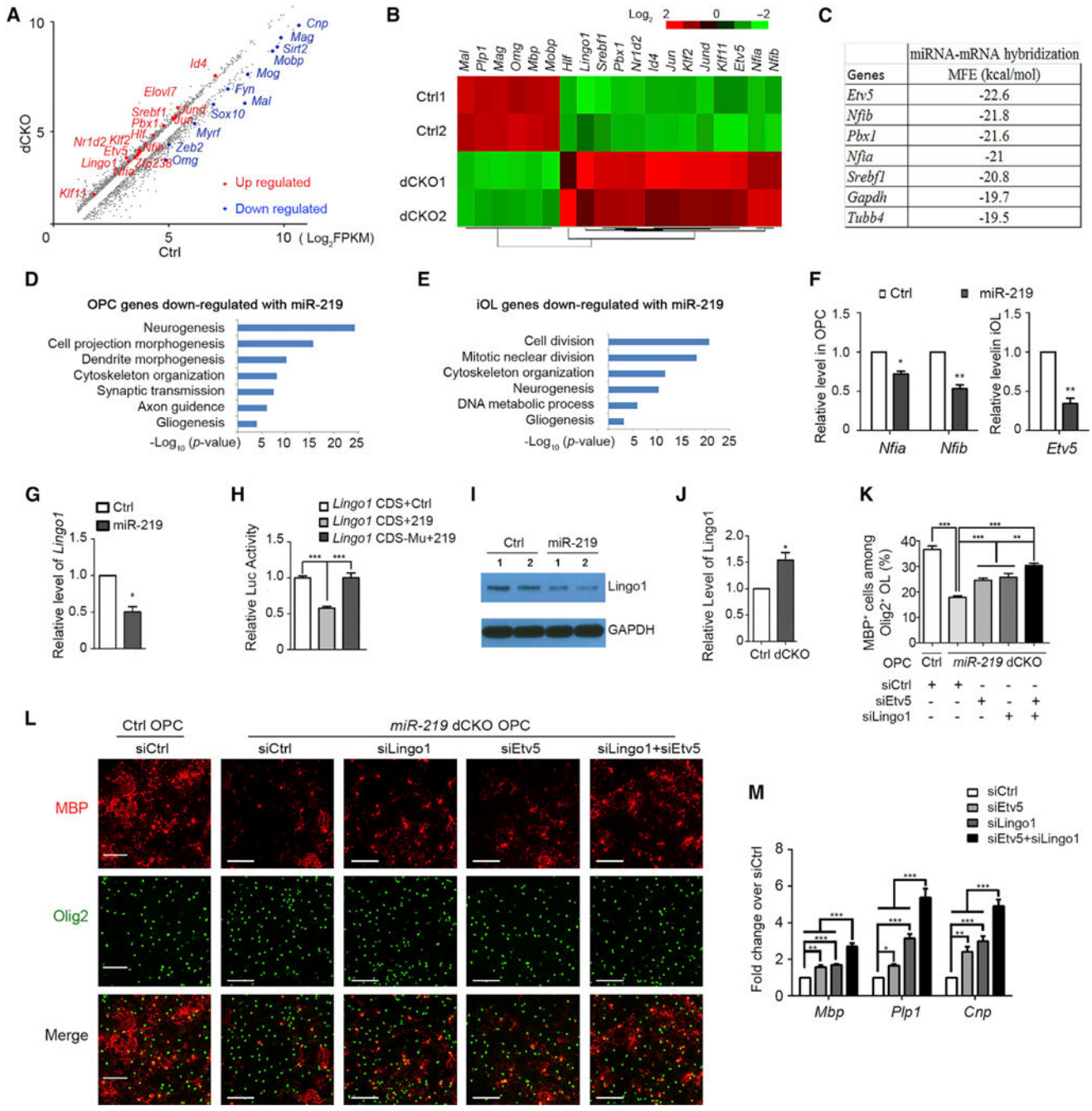

Figure 6. Stage-Specific Targeting of OL Differentiation Inhibitors by miR-219

(A and B) Differentially expressed transcripts between P12 wild-type and *miR-219*-dCKO optic nerves are shown by (A) scatterplot and (B) heatmap.

(C) Predicted miRNA-mRNA hybridization minimum free energies (MFEs) between candidate miR-219-targeted transcription factors and non-targeted housekeepers Gapdh and Tubb4.

(D and E) GO analyses of the biological processes for downregulated transcripts in miR-219-mimic-treated OPCs (D) or immature OLs (iOL) under differentiation media for 1 day (E) compared with controls.

(F) qRT-PCR analysis of *Nfia* and *Nfib* in OPC and *Etv5* in iOL transfected with Ctrl or miR-219 mimics. $n = 3$ experiments. *p < 0.05, **p < 0.01, Student's t test.
(G) qRT-PCR analysis of *Lingo1* in OPCs transfected with Ctrl or miR-219 mimic. $n = 3$ independent transfections. *p < 0.05, Student's t test.
(H) Relative luciferase activity of reporter constructs carrying the *Lingo1* segments containing the *miR-219* binding sites or the mutated binding sites. $n = 3$ transfections. ***p < 0.001, Student's t test.
(I) Immunoblotting for Lingo1 in OPCs 2 days after transfection with control or miR-219 mimic.
(J) qRT-PCR analysis of *Lingo1* in P12 Ctrl and *miR-219*-dCKO optic nerves. $n = 3$ animals/genotype. *p < 0.05, Student's t test.
(K) Quantification of the percentage of MBP+ cells among $Olig2^+$ cells in Ctrl and *miR-219*-dCKO OLs treated with siCtrl, siLingo1, siEtv5, or siLingo1 plus siEtv5. $n = 3$ transfections. **p < 0.01, ***p < 0.001, one-way ANOVA with Tukey's multiple-comparison test.
(L) OPCs isolated from Ctrl and *miR-219*-dCKO animals were transfected with scrambled control siRNA (siCtrl), siLingo1, siEtv5, or siLingo1 plus siEtv5 and were cultured in differentiating media for 3 days. Cells were stained for MBP (red) and Olig2 (green). Scale bars: 100 μm.
(M) Quantification of myelin gene expression in Ctrl and *miR-219*-dCKO OLs treated with siCtrl, siLingo1, siEtv5, or siLingo1 plus siEtv5. $n = 3$ transfections. *p < 0.05, **p < 0.01, ***p < 0.001, one-way ANOVA with Tukey's multiple-comparison test.
Data in (F–H), (J), (K), and (M) are presented as means ± SEM.

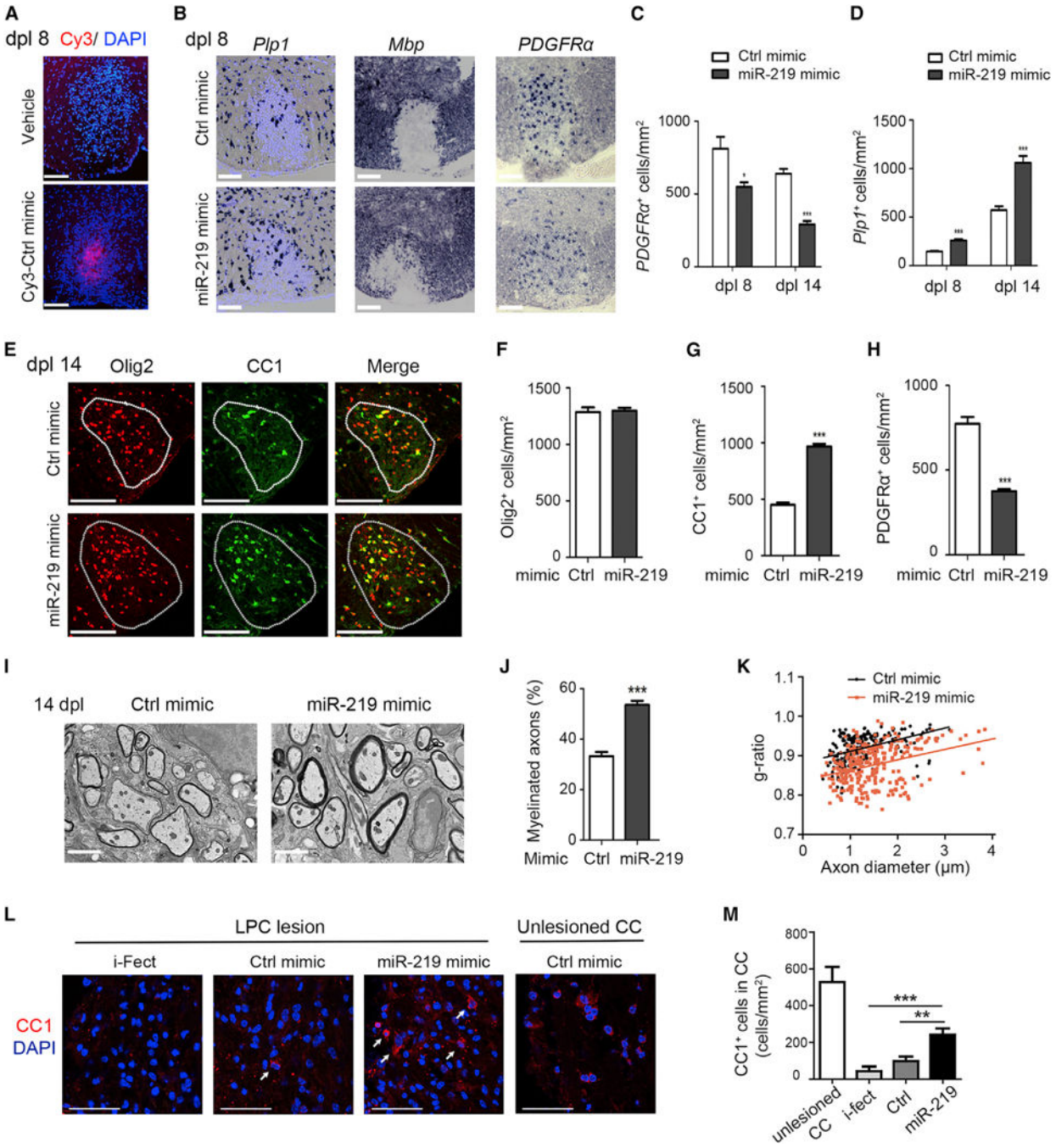

Figure 7. miR-219 Mimics Enhance Remyelination in LPC-Induced Demyelinated Lesions

(A) Confocal images show delivery of vehicle and Cy3-tagged control miRNA to the lesion of the spinal cord at dpl 8. Scale bars: 100 μm.

(B) RNA insitu hybridization for *Plp1*, *Mbp*, and *PDGFRα* in representative LPC lesions in spinal cords of the mice treated with control miRNA mimic (Ctrl mimic) or miR-219 mimic at dpl 8. DAPI counterstaining is shown in blue in the left panels. Scale bars: 100 μm.

(C and D) Number of *PDGFRα*$^+$ (C) or *Plp*$^+$ (D) cells per mm^2 in the LPC lesions in spinal cords of the mice treated with Ctrl or miR-219 mimic at dpl 8 and dpl 14. At dpl 8, $n = 6$ and

7 animals treated with Ctrl and miR-219 mimics, respectively; at dpl 14, n = 8 animals/treatment. *p < 0.05, ***p < 0.001, Student's t test.

(E) Immunostaining forCC1and Olig2 in LPC lesions (dashed circle) at dpl14 in the spinal cord of the mice treated with CtrlormiR-219 mimic. Scale bars: 100 μm.

(F–H) Quantification of (F) $Olig2^+$ cells, (G) $CC1^+$ OLs, and (H) $PDGFR\alpha^+$ OPCsinLPC lesions in the spinal cord of the mice treated with Ctrl or miR-219 mimic at dpl 14. $n = 8$ animals/treatment. ***p < 0.001, Student's t test.

(I) EM images of the LPC lesion in ventral spinal cords from Ctrl or miR-219-mimic-treated mice at dpl 14. Scale bars: 2 μm.

(J) Percentage of remyelinated axons in LPC lesions in the spinal cords from mice treated with Ctrl or miR-219 mimic at dpl 14. $n = 4$ animals/treatment. ***p < 0.001, Student's t test.

(K) Scatterplot of *g* ratio versus axon diameter at dpl 14 in LPC lesions of mice treated with Ctrl or miR-219 mimic. $n = 4$ animals/genotype. p < 0.001, Student's t test.

(L) Immunostaining for $CC1^+$ OLs (arrows) in LPC lesions of mice infused intranasally with vehicle (i-Fect), scrambled control miRNA (Ctrl mimic), miR-219 mimic, and unlesioned corpus callosum of mice treated with Ctrl mimic. Scale bars: 50 μm.

(M) Quantification of CC1+ cells per area (mm^2) in LPC lesions and unlesioned CC. $n = 3$ per group. **p < 0.01 and ***p < 0.001, one-way ANOVA with Tukey's multiple-comparison test.

Data in (C), (D), (F–H), (J), and (M) are presented as means ± SEM.

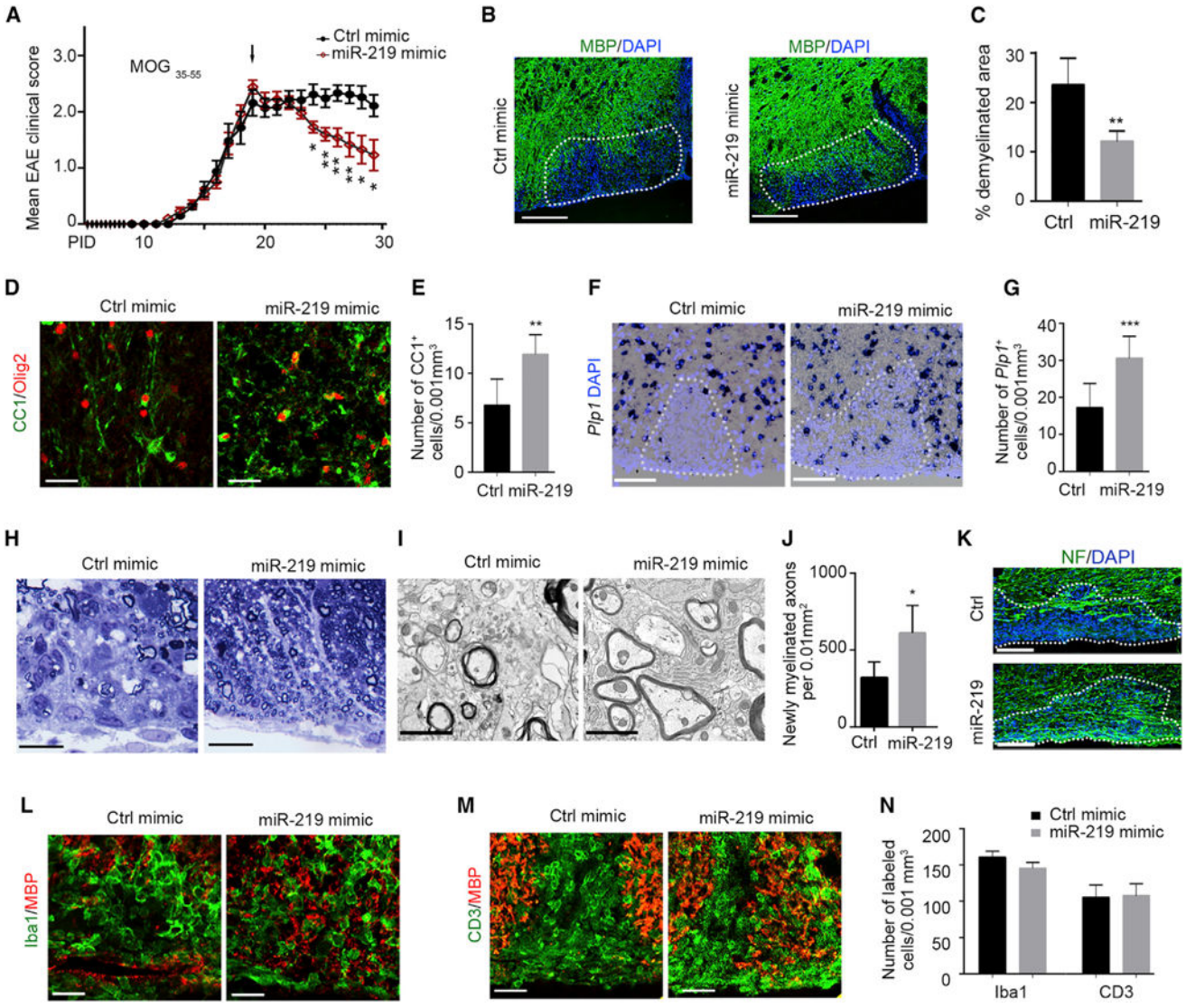

Figure 8. Therapeutic Efficacy of miR-219 Mimic in the EAE Model of MS

(A) Clinical score in chronic progressive MOG35-55-induced EAE mice treated with control and miR-219 mimic daily for 5 days beginning at the peak of disease at post-immunization day (PID) 19 (black arrow). $n = 17$ animals for each control and miR-219 treated group. *p < 0.05, **p < 0.01, Student's t test.

(B) Immunostaining for MBP in lesion areas (dashed outline) at PID 29 in the lumbar spinal cord of mice treated with control (Ctrl) or miR-219 mimics. Scale bars: 100 μm.

(C) Percentage of the white matter region of the lumbar spinal cords that were demyelinated in mice treated with Ctrl or miR-219 mimics at PID 29. $n = 5$ animals per group. **p < 0.01, Student's t test.

(D) Immunostaining for CC1 and Olig2 in lesion areas at PID 29 in the lumbar spinal cord of mice treated with control or miR-219 mimic. Scale bars: 25 μm.

(E) Quantification of $CC1^+$ cell density in lesions at PID 29 in the lumbar spinal cord of mice treated with control or miR-219 mimic.$n = 7$ mice per group. **p < 0.01, Student's t test.

(F) RNA in situ hybridization for *Plp1* in lesion areas (dashed outline) at PID 29 in lumbar spinal cords of mice treated with control or miR-219 mimic. DAPI counterstaining is shown in red. Scale bars: 100 μm.

(G) The $Plp1^+$ cell density in the lesions at PID 29 in lumbar spinal cords of mice treated with control or miR-219 mimics. $n = 6$ animals per groups treated with control and miR-219 mimics, respectively. ***$p < 0.001$, Student's t test.

(H) Toluidine blue staining in the lesion areas at PID 29 in spinal cords of mice treated with control or miR-219 mimics. Scale bars: 20 μm.

(I) EM images of the lesion areas at PID 29 in ventral spinal cords from control or miR-219-mimic-treated mice. Scale bars: 2 μm.

(J) Average newly myelinated axons per area (0.01 mm^2) in demyelinating lesions at PID 29 in the lumbar spinal cord of mice treated with control or miR-219 mimics. $n = 5$ mice per group. *$p < 0.05$, Student's t test.

(K) Immunostaining for neurofilament M (NF) in lesion areas (dashed circle) at PID 29 in the lumbar spinal cord of mice treated with Ctrl or miR-219 mimic. Scale bars: 100 μm.

(L and M) Immunostaining for MBP with Iba1 (L) and CD3 (M) in lesion areas at PID 29 in the lumbar spinal cord of mice treated with Ctrl or miR-219 mimic. Scale bars: 25 μm.

(N) Quantification of $Iba1^+$ and $CD3^+$ cell density in lesions at PID 29 in the lumbar spinal cord of mice treated with Ctrl or miR-219 mimic (right). $n = 8$ mice per group (Student's t test).

Data in (A), (C), (E), (G), (J), and (N) are presented as means ± SEM.